AN ABSTRACT OF THE THESIS OF

THEODORE WILES CANNON for the Ph. D. in PHYSICS
(Name) (Degree) (Major)

Date thesis is presented November 29, 1965

Title PERTURBED DIRECTIONAL CORRELATION IN Ta-181

Abstract approved Redacted for Privacy
(Major professor)

The effect of a static quadrupole interaction on the 133-482 Kev gamma-gamma angular correlation in Ta^{181} has been studied by the delayed-coincidence method. Using a source of Hf^{181} in polycrystalline hafnium metal, the anisotropy was measured as a function of the time between the formation and decay of the 482 Kev state with a fast-slow coincidence spectrometer. The anisotropy as a function of time clearly revealed fluctuations arising from the reorientation of the nuclear spin due to coupling of the quadrupole moment of the 482 Kev state with the electric field gradients of the crystals. The interaction strength evaluated on the basis of the theory for axially symmetric gradients was $\omega_o = 299 \pm 8$ Mc/sec. Evidence for the presence of a rhombic (non-axially symmetric) electric interaction was observed in the departure of the results from the predictions for the axially symmetric case. The results are, however, in agreement with the theory for rhombic interactions if the electric field gradient in the hafnium crystals is assumed to have an asymmetry parameter

$\eta = 0.30 \pm 0.03$, and in addition, if a normal frequency distribution of full width at half-maximum equal to 10% is used to describe the variation of the field gradient from site to site. Further, using the evidence from Coulomb excitation for the strong deformation of the tantalum nucleus, it was determined that the quadrupole moment of the 482 Kev state is $Q = (2.53 \pm 0.10) \times 10^{-24} cm^2$. This allows the calculation of the field gradient magnitudes in metallic hafnium. which yields $V_{zz} = \pm (5.18 \pm 0.27) \times 10^{17} V/cm^2$, $V_{yy} = \mp (3.37 \pm 0.19) \times 10^{17} V/cm^2$, and $V_{xx} = \mp (1.81 \pm 0.25) \times 10^{17} V/cm^2$.

The effect of a combined magnetic dipole and electric quadrupole interaction was also studied for the 133-482 Kev correlation using external fields of 4.8 kilogauss and 8.3 kilogauss applied perpendicular to the plane of the detectors. Agreement with the theory for the case of mixed interactions was attained by assuming values of $y = \frac{6\omega_H}{\omega_o}$ corresponding to the values of applied magnetic field, as well as an asymmetry parameter for the electric field gradient of 0.30 and a gaussian distribution of 10% width as in the zero field case. It is concluded that it is very difficult to measure nuclear magnetic moments by delayed differential angular correlation methods in solid sources with electric quadrupole and magnetic dipole interactions of the same order of magnitude if an appreciable distribution in quadrupole interaction frequencies exists within the sample.

PERTURBED DIRECTIONAL CORRELATION IN Ta-181

by

THEODORE WILES CANNON

A THESIS

submitted to

OREGON STATE UNIVERSITY

in partial fulfillment of
the requirements for the
degree of

DOCTOR OF PHILOSOPHY

June 1966

APPROVED:

Redacted for Privacy

Professor of Department of Physics

Redacted for Privacy

Acting Chairman of Department of Physics

Redacted for Privacy

Dean of Graduate School

Date thesis is presented November 29, 1965

Typed by Muriel Davis

TABLE OF CONTENTS

	Page
INTRODUCTION	1
PERTURBED DIRECTIONAL CORRELATION WITH NON-AXIALLY SYMMETRIC ELECTRIC QUADRUPOLE INTERACTION	4
Theory	4
Introduction	4
Perturbed Angular Correlation-General Case	4
Axially and Non-axially Symmetric Electric Field Interactions	12
Axially Symmetric Case	19
Non-axially Symmetric Case	20
Apparatus	21
Description of Coincidence Spectrometer	21
Development Work on Coincidence Spectrometer	24
Experimental Measurements	28
Results and Conclusions	32
PERTURBED DIRECTIONAL CORRELATION WITH COMBINED MAGNETIC DIPOLE AND NON-AXIALLY SYMMETRIC ELECTRIC QUADRUPOLE INTERACTION	44
Theory	44
Introduction	44
The Magnetic Dipole Interaction	45
The Combined Magnetic Dipole and Non-axially Symmetric Electric Quadrupole Interaction Hamiltonian	46
Calculation of Anisotropy for the Mixed Case	56
Experimental Measurement	58
Results and Conclusions	60
BIBLIOGRAPHY	73

TABLE OF CONTENTS (continued)

	Page
APPENDIX	77
Frequency Fold for the Mixed Case	77
Derivation of $W(\theta, t)$ with Solid Angle Corrections	78
No Applied Magnetic Field	78
Applied Magnetic Field	81

LIST OF FIGURES

Figure		Page
1	Decay of an excited nucleus by two-gamma cascade	5
2	Vectors defining the positions of the nuclear charges e_c and extranuclear charges e_p	13
3	Arrangement of detected gamma radiations and crystalline field gradients for $\eta \neq 0$ case	15
4	Rotation of coordinate system of a crystal through α_1, β_1, and γ	18
5	Block diagram of delayed coincidence spectrometer	23
6	Energy levels and decay scheme for hafnium-181	29
7	The anisotropy of the 133-482 kilovolt gamma-gamma cascade obtained with a polycrystalline source	34
8	Comparison of the measured anisotropy with a rhombic interaction using an asymmetry parameter $\eta = 0.30$	35
9	Comparison of the measured anisotropy with a rhombic interaction including a normal frequency distribution having a full width at half-maximum of 10%	36
10	Arrangement of detected gamma radiations, magnetic field vector, and crystalline field gradients for $\eta \neq 0$, $y \neq 0$ case	47
11	Theoretical values of anisotropy A(t) for an electric quadrupole interaction strength of 299 Mc/Sec and asymmetry parameter $\eta = 0.30$ for $0.460 \leq y \leq 0.855$	63
12	Theoretical values of anisotropy A(t) for an electric quadrupole interaction strength of 299 Mc/Sec and asymmetry parameter $\eta = 0.30$ for $0.795 \leq y \leq 1.476$	64

LIST OF FIGURES (continued)

Figure		Page
13	Time dependent anisotropy of the 133-482 kilovolt gamma cascade in polycrystalline hafnium metal with applied magnetic field of 4.8 kilogauss. The dashed curve represents the uncorrected theory for asymmetry parameter $\eta = 0$ and $y = \frac{\omega_H}{\omega_E} = 0.585$, and the solid curve represents the same theory with corrections for solid angles subtended by the detectors as well as the prompt response of the spectrometer	66
14	Time dependent anisotropy of the 133-482 kilovolt gamma cascade in polycrystalline hafnium metal with applied magnetic field of 8.3 kilogauss. The dashed curve represents the uncorrected theory for asymmetry parameter $\eta = 0$ and $y = \frac{\omega_H}{\omega_E} = 0.877$ and the solid curve represents the same theory with corrections for solid angles subtended by the detectors as well as the prompt response of the spectrometer	68
15	Time dependent anisotropy of the 133-482 kilovolt gamma cascade in polycrystalline hafnium metal with applied magnetic field of 4.8 kilogauss. The dashed curve represents the uncorrected theory for asymmetry parameter $\eta = 0.30$ and $y = 0.591$ and the solid curve represents the same theory with corrections for solid angles subtended by the detectors as well as the prompt response of the spectrometer and a gaussian distribution in ω_E of width $\delta = 10\%$	70
16	Time dependent anisotropy of the 133-482 kilovolt gamma cascade in polycrystalline hafnium metal with applied magnetic field of 8.3 kilogauss. The dashed curve represents the uncorrected theory for asymmetry parameter $\eta = 0.30$ and $y = 1.022$ and the solid curve represents the same theory with corrections for solid angles subtended by	

LIST OF FIGURES (continued)

Figure		Page
	the detectors as well as the prompt response of the spectrometer and a gaussian distribution in ω_E of width $\delta = 10\%$	72
Appendix Figure		
A1	Map of ranges of y/y_o and x for which $a^s_{\nu_1\nu_2}$ were calculated to make the frequency distribution fold for each y_o value	79

PERTURBED DIRECTIONAL CORRELATION IN Ta-181

INTRODUCTION

In an angular correlation experiment, one studies the decay of nuclei which emit two particles or radiations in rapid succession. The relative probability $W(\theta)d\Omega$ that the second radiation or particle will be emitted into the differential solid angle $d\Omega$ at an angle θ with respect to the direction of the first radiation or particle is determined. We shall restrict ourselves to gamma radiations in this discussion, although several other types of experiments are done in practice e. g. beta-gamma and alpha-gamma angular correlations.

Angular correlation experiments are performed for the purpose of determining properties of nuclei and their radiations. These properties include spins, multipolarities, mixing ratios, and relative parities.

The assumption is often made that, during the time which elapses between emission of the first and second radiations, the nucleus is unaffected by local electric or magnetic fields or by atomic collisions. Such a nucleus is said to be "free." Such an assumption is not always valid, for in no situation is the nucleus entirely free of the influence of fields or collisions. The effect of these fields and collisions is to reorient the nuclear spins. In many cases, angular

correlations are found to depend on the physical and chemical nature of the source. The extent to which this occurs depends on the magnitude of the influencing factors, as well as the length of the time delay between emission of the first and second radiations. One must be aware that the nucleus can not always be considered to be free in an angular correlation experiment, and discrepancies between observed results and those predicted by theory may sometimes be accounted for by these perturbing effects.

On the other hand, this very influence of fields on the nuclear spin orientation may itself be useful for determining certain properties of the nucleus or its environment. An angular correlation experiment in which reorientation effects are detectable is called a perturbed angular or perturbed directional correlation experiment. The perturbing fields may arise either from the atomic, molecular, or crystalline structure of the source, or may be applied externally. Perturbed angular correlation experiments have been performed to determine, among other things, nuclear g-factors (7), nuclear quadrupole interactions (33), the electric field gradients in various metals and alloys (16, 17), and the internal magnetic field in certain rare earth elements (9).

It is the purpose of this thesis to describe two perturbed angular correlation experiments performed on a gamma-gamma cascade whose origin is a nucleus immersed in polycrystalline hafnium metal.

The first experiment was done to determine the magnitude, as well as to estimate the spatial variation of the magnitude of the electric field gradient components in the hafnium crystals. The second experiment was a measurement of the angular distribution of radiation with the same polycrystalline source placed in an externally applied magnetic field. The results of this experiment were compared with computer calculations based on the theory for the influence of combined magnetic dipole and non-axially symmetric electric quadrupole interactions on the angular distribution. Comparison of theory with experiment was used as a test of the theory and the usefulness of its inherent assumptions.

PERTURBED DIRECTIONAL CORRELATION WITH NON-AXIALLY SYMMETRIC ELECTRIC QUADRUPOLE INTERACTION

Theory

Introduction

The theory for the influence of perturbing interactions on angular correlations has been developed by several authors. The general theory of perturbed and unperturbed directional correlations has been treated by Alder (2). Abragam and Pound (1) have reformulated the theory to include time-dependent as well as static interactions in the intermediate nuclear state. Theoretical work on the influence of a combined magnetic dipole and axially symmetric electric quadrupole interaction on directional correlations has been done by Alder, Matthias, Schneider, and Steffen (3, 22), while the case of a combined magnetic dipole and non-axially symmetric electric quadrupole interaction has been treated by Matthias, Olsen, Schneider, and Steffen (21, 23). We wish to formulate the theory for the axially and non-axially symmetric electric quadrupole interactions alone, using the notation of Rose (29).

Perturbed Angular Correlation-General Case

Consider a nucleus which decays from states A to B through emission of γ_1 and from states B to C through emission of γ_2.

These two radiations will be emitted in directions $\vec{k}_1$ and $\vec{k}_2$ whose spherical coordinates are defined as shown in Figure 1.

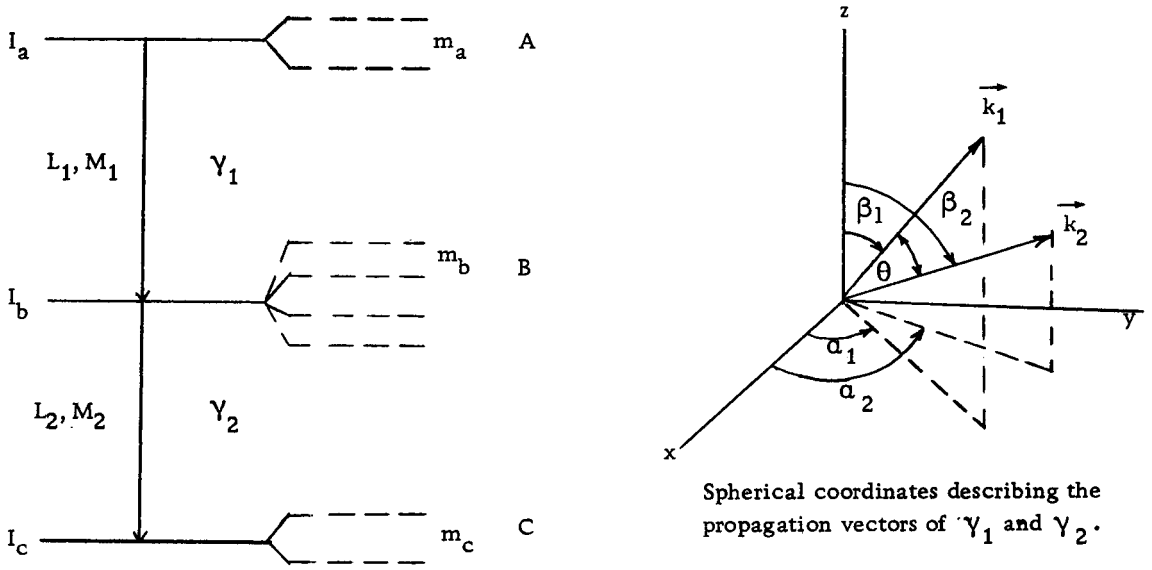

Figure 1. Decay of an excited nucleus by two-gamma cascade.

Let $W(\theta, 0) = W(\vec{k}_1, \vec{k}_2; 0)$ be the probability of γ_2 being emitted in direction $\vec{k}_2$ making an angle θ with the direction $\vec{k}_1$ of γ_1. For the unperturbed angular correlation, $W(\vec{k}_1, \vec{k}_2; 0)$ is given by (29, p. 169)

$$W(\vec{k}_1, \vec{k}_2; 0) = \sum_{m_a, m_c} \left| \sum_{m_b} \langle I_c m_c | H_2 | I_b m_b \rangle \langle I_b m_b | H_1 | I_a m_a \rangle \right|^2 \qquad (1)$$

where H_1 and H_2 represent interaction Hamiltonians for emission

of γ_1 in direction $\vec{k}_1$ and γ_2 in direction $\vec{k}_2$, respectively. The state functions describing a particular state are denoted by $|Im\rangle$ where I and m, with appropriate subscripts, denote the angular momentum (spin) and projection quantum numbers characterizing that state. The matrix elements $\langle I_i m_i | H_k | I_j m_j \rangle$ are probability amplitudes for the various possible transitions between degenerate substates.

Expanding equation (1), we obtain

$$W(\vec{k}_1, \vec{k}_2; 0) = \sum_{m_a, m_c} \sum_{m_b, m_b'} \sum_{m_b'', m_b'''} \langle I_c m_c | H_2 | I_b m_b'' \rangle \langle I_c m_c | H_2 | I_b m_b''' \rangle^* \tag{2}$$

$$\times \langle I_b m_b | H_1 | I_a m_a \rangle \langle I_b m_b' | H_1 | I_a m_a \rangle^* \delta_{m_b m_b''} \delta_{m_b' m_b'''}.$$

In the absence of an extranuclear perturbation which would reorient I_b, the initial states of the second radiation $|I_b m_b''\rangle$ and $|I_b m_b'''\rangle$ are identical to the final states of the first radiation $\langle I_b m_b|$ and $\langle I_b m_b'|$ respectively.

We now assume the presence of an interaction of the nucleus in its intermediate state with some extranuclear field. This interaction is described by the Hamiltonian H_Q and acts during the time t between emission of γ_1 and γ_2. During this time, states $\langle I_b m_b|$ and $\langle I_b m_b'|$ change to different states $|I_b m_b''\rangle$ and $|I_b m_b'''\rangle$, respectively, due to the perturbation. We may represent

this change by the operator $\Gamma(t)$ which describes the evolution of the intermediate state vectors. The perturbed angular correlation now becomes

$$W(\vec{k}_1, \vec{k}_2; t) = \sum_{m_a, m_c} \sum_{m_b, m_b'} \langle I_c m_c | H_2 \Gamma(t) | I_b m_b \rangle \langle I_c m_c | H_2 \Gamma(t) | I_b m_b' \rangle^*$$

$$\times \langle I_b m_b | H_1 | I_a m_a \rangle \langle I_b m_b' | H_1 | I_a m_a \rangle^* . \tag{3}$$

The final states form a complete set, and the state vectors can be represented by

$$\Gamma(t) | I_b m_b \rangle = \sum_{m_b''} \langle I_b m_b'' | \Gamma(t) | I_b m_b \rangle | I_b m_b'' \rangle \tag{4}$$

and a similar expression holds for $\Gamma(t) | I_b m_b' \rangle^*$. This allows us to write equation (3) in the form

$$W(\vec{k}_1, \vec{k}_2; t) = \sum_{m_a, m_c} \sum_{m_b, m_b''} \sum_{m_b', m_b'''} \langle I_c m_c | H_2 | I_b m_b'' \rangle$$

$$\times \langle I_b m_b'' | \Gamma(t) | I_b m_b \rangle \langle I_c m_c | H_2 | I_b m_b''' \rangle^* \tag{5}$$

$$\times \langle I_b m_b''' | \Gamma(t) | I_b m_b' \rangle^* \langle I_b m_b | H_1 | I_a m_a \rangle \langle I_b m_b' | H_1 | I_a m_a \rangle^* .$$

Making use of the identities (29, p. 174)

$$\sum_{m_a} \langle I_b m_b | H_1 | I_a m_a \rangle \langle I_b m_b' | H_1 | I_a m_a \rangle^*$$

$$= \sum_{\nu_1} (-)^{m_b' - I_b} C(I_b I_b \nu_1; m_b, -m_b', s_1)\, D^{\nu_1}_{m_b - m_b', 0}(\alpha_1 \beta_1 0) B_{\nu_1}(\gamma_1)$$

$$\sum_{m_c} \langle I_c m_c | H_2 | I_b m_b'' \rangle \langle I_c m_c | H_2 | I_b m_b''' \rangle^*$$

$$= \sum_{\nu_2} (-)^{m_b'' - I_b} C(I_b I_b \nu_2; m_b'', -m_b''', s_2)\, D^{\nu_2}_{m_b''' - m_b'', 0}(\alpha_2 \beta_2 0) B_{\nu_2}(\gamma_2)$$

we obtain

$$W(\vec{k}_1, \vec{k}_2; t) = \sum_{\nu_1, \nu_2} \sum_{s_1, s_2} (-)^{s_2} G^{s_1 s_2}_{\nu_1 \nu_2}(t)\, D^{\nu_1}_{s_1, 0}(\alpha_1 \beta_1 0)$$

$$D^{\nu_2}_{-s_2, 0}(\alpha_2 \beta_2 0)\, B_{\nu_1}(\gamma_1)\, B_{\nu_2}(\gamma_2) \tag{6}$$

where the time dependence of $W(\vec{k}_1, \vec{k}_2; t)$ is contained in $G^{s_1 s_2}_{\nu_1 \nu_2}(t)$, defined as the perturbation factor and given by the expression

$$G^{s_1 s_2}_{\nu_1 \nu_2}(t) = \sum_{m_b, m_b''} (-)^{m_b' + m_b'' - 2I_b} C(I_b I_b \nu_1;\ m_b, -m_b', s_1)$$

$$C(I_b I_b \nu_2; m_b'', -m_b''', s_2) \langle I_b m_b'' | \Gamma(t) | I_b m_b \rangle \langle I_b m_b''' | \Gamma(t) | I_b m_b' \rangle^*. \tag{7}$$

In the above two equations $D^{\nu_1}_{s_1,0}(\alpha_1\beta_1 0)$ and $D^{\nu_2}_{-s_2,0}(\alpha_2\beta_2 0)$ are rotation matrix elements affecting rotations through the Euler angles defined in Figure 1; $B_{\nu_1}(\gamma_1)$ and $B_{\nu_2}(\gamma_2)$ are constant factors which are independent of the projection quantum numbers for any $\gamma_1 - \gamma_2$ pair, but are dependent upon the L and I which are characteristic of the transition, L being the multipolarity of the transition. $C(I_b I_b \nu_1; m_b, -m_b', s_1)$ is a Clebsch-Gordon coefficient which vanishes unless the vector triple $\Delta(I_b, I_b, \nu_1)$ forms a triangle and $s_1 = m_b - m_b'$, and similarly for $C(I_b I_b \nu_2; m_b'', -m_b''', s_2)$. If the perturbation is absent, $\Gamma(t) = 1$ and the orthogonality relations for the Clebsch-Gordon coefficients allow us to write $G^{s_1 s_2}_{\nu_1\nu_2}(t) = \delta_{s_1 s_2}\delta_{\nu_1\nu_2}$. Similarly, as we approach the limit $t \to 0$ during which a perturbation has had no time to act, we find $\lim_{t\to 0} G^{s_1 s_2}_{\nu_1\nu_2} = \delta_{s_1 s_2}\delta_{\nu_1\nu_2}$. Using the addition theorem of spherical harmonics on the product of the D's, one may write for either of these cases

$$W(\theta, 0) = \sum_{\nu} B_{\nu}(\gamma_1) B_{\nu}(\gamma_2) P_{\nu}(\cos\theta) \tag{8}$$

which corresponds to the expression of Biedenharn and Rose (6, p.746) for $\gamma - \gamma$ correlations for pure multipoles

$$W(\theta) = \sum_{\nu} A_{\nu} P_{\nu}(\cos\theta)$$

where P_{ν} = the Legendre polynomial of order ν and argument $\cos\theta$, and $A_{\nu} = F_{\nu}(L_1 I_a I_b) F_{\nu}(L_2 I_c I_b)$ with

$$F_\nu(L_1 I_a I_b) = (-)^{I_a - I_b - 1} (2I_b+1)^{\frac{1}{2}} (2L_1+1)$$

$$\times \; C(L_1 L_1 \nu;\; 1, -1, 0)\, W(I_b I_b L_1 L_1;\; \nu I_a) \qquad (10)$$

and a similar expression holds for $F_\nu(L_2 I_c I_b)$. Values of F_ν are tabulated for a number of spins (See Ref. 13 for example).

It can be shown on the basis of parity arguments that ν can only have even integer values (6, p. 742). ν_{max} must be the smallest of the integers $2I_b$, $2L_1$, or $2L_2$, as may be seen by noting that the triangle rules $\Delta(I_b I_b \nu)$, $\Delta(L_1 L_1 \nu)$, and $\Delta(L_2 L_2 \nu)$ must hold for the Clebsch-Gordon coefficients in equations (7) and (10).

The evolution operator $\Gamma(t)$ must satisfy the equation

$$\dot{\Gamma}(t) = (-i/\hbar)\, H_Q \Gamma(t) .$$

For the case of "static" interactions, H_Q is time independent and we have

$$\Gamma(t) = e^{-(i/\hbar) H_Q t} \qquad (11)$$

If the perturbation is caused by an external field that can be described classically, the matrix elements of $\Gamma(t)$ can be expressed in m representation. If U = the unitary operator which diagonalizes the interaction Hamiltonian, then

$$U H_Q U^{-1} = E$$

where E is the diagonal matrix with elements E_{m_z}, the energy eigenvalues.

By expansion of exponentials

$$U e^{(-i/\hbar)H_Q t} U^{-1} = e^{(-i/\hbar)Et}$$

and substituting from equation (11) above

$$\Gamma(t) = U^{-1} e^{-(i/\hbar)Et} U \quad . \tag{12}$$

Substituting equation (12) into the evolution matrix elements, we get the matrix elements

$$\langle I_b m_b'' | \Gamma | I_b m_b \rangle = \langle I_b m_b'' | U^{-1} e^{-(i/\hbar)Et} U | I_b m_b \rangle$$

$$= \sum_{m_z} \langle I_b m_b'' | U^{-1} | I_b m_z \rangle \langle I_b m_z | e^{-(i/\hbar)Et} | I_b m_z \rangle$$

$$\times \langle I_b m_z | U | I_b m_b \rangle$$

$$= \sum_{m_z} \langle I_b m_z | U | I_b m_b'' \rangle^* \langle I_b m_z | U | I_b m_b \rangle e^{-(i/\hbar)E_{m_z} t} \tag{13}$$

where $\langle I_b m_z | U | I_b m_b \rangle$ are the matrix elements of the unitary operator which diagonalizes H_Q. The perturbation coefficient now becomes

$$G^{s_1 s_2}_{\nu_1 \nu_2}(t) = \sum_{m_z, m_z'} \sum_{m_b, m_b''} (-)^{m_b' + m_b'' - 2I_b} C(I_b I_b \nu_1; m_b, -m_b', s_1) \tag{14}$$

$$\times C(I_b I_b \nu_2; m_b'', -m_b''', s_2) \langle I_b m_z | U | I_b m_b'' \rangle^* \langle I_b m_z | U | I_b m_b \rangle$$

$$\times \langle I_b m_z' | U | I_b m_b''' \rangle \langle I_b m_z' | U | I_b m_b' \rangle^* e^{-i/\hbar(E_{m_z} - E_{m_z'})t} .$$

Inspection of equation (14) shows that it is necessary to find the eigenvalues E_{m_z} and $E_{m_z'}$ as well as the matrix elements $\langle I_b m_z | U | I_b m_b'' \rangle$ etc. in order to evaluate $G^{s_1 s_2}_{\nu_1 \nu_2}$ for a particular experimental situation. We will now proceed to calculate $G^{s_1 s_2}_{\nu_1 \nu_2}$ for two important cases.

Axially and Non-axially Symmetric Electric Field Interactions

Let us now compute the Hamiltonian for the case of a non-axially symmetric electric quadrupole interaction. We will then show how this Hamiltonian is used in connection with equation (14) to compute the perturbation factors for this case.

The interaction Hamiltonian has been shown (22, p. 263) to be

$$\mathcal{H}_{el} = \frac{4\pi}{5} \sum_q (-)^q T_q^{(k)} V_{-q}^{(k)} = \sum_{k=0}^{\infty} \frac{4\pi}{2k+1} T^{(k)} V^{(k)} \tag{15}$$

where

$$T_q^{(k)} = \sum_p e_p r_p^k Y_{k,q}(\theta_p, \phi_p) \tag{16}$$

$$V_q^{(k)} = \sum_c e_c \frac{1}{r_c^{k+1}} Y_{k,q}(\theta_c, \phi_c) \quad . \tag{17}$$

$T^{(k)}$ and $V^{(k)}$ are the tensor operators of the nuclear moments and extranuclear field, respectively. Equation (16) is a sum over all nuclear charges e_p and equation (17) is a sum over all

extranuclear charges e_c. The position vectors of these charges are defined in Figure 2.

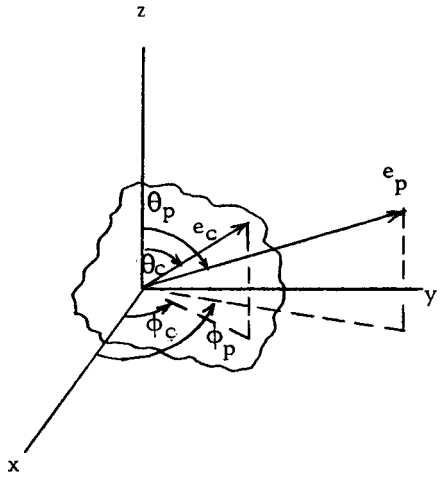

Figure 2. Vectors defining the positions of the nuclear charges e_c and extranuclear charges e_p.

Ignoring all but quadrupole terms (34, p. 19),

$$\mathcal{H}_{el} = \frac{4}{5}\pi\, T^{(2)} V^{(2)} = \frac{4\pi}{5} \sum_q (-)^q\, T_q^{(2)} V_{-q}^{(2)} .$$

Writing the quadrupole interaction matrix elements

$$\langle I_m | \mathcal{H}_{el} | I_m' \rangle = \frac{4\pi}{5} \sum_q (-)^q \langle I_m | T^{(2)} | I_m' \rangle\, V_{-q}^{(2)}$$

and using the Wigner-Eckart theorem (29, p. 85)

$$\langle I_m | \mathcal{H}_{el} | I_m' \rangle = \frac{4\pi}{5} (-)^q C(I2I;\, m, q, m')\, (I \,||\, T_q \,||\, I)\, V_{-q}^{(2)} \qquad (18)$$

where q is determined by m and m', so the sum over q is dropped. Note that because of properties of the Clebsch-Gordon

coefficients $|q| \leq 2$ and since $q = m - m'$, $m - m' \leq 2$.

The electrostatic field of the crystal is known in some coordinate system S. The components of the electric field tensor $V_1^{(2)}$ as computed from equation (17) are

$$V_0^{(2)} = \frac{1}{4} \sqrt{\frac{5}{\pi}} \; V_{zz}$$

$$V_{\pm 1}^{(2)} = \mp \frac{1}{2} \sqrt{\frac{5}{6\pi}} \; (V_{xz} \pm i \, V_{yz})$$

$$V_{\pm 2}^{(2)} = \frac{1}{4} \sqrt{\frac{5}{6\pi}} \; (V_{xx} - V_{yy} \pm 2i \, V_{xy}) \, .$$

The S coordinate system may be chosen such that the mixed derivatives vanish, leaving us with

$$V_0^{(2)} = \frac{1}{4} \sqrt{\frac{5}{\pi}} \; V_{zz}$$

$$V_{\pm 1}^{(2)} = 0 \tag{19}$$

$$V_{\pm 2}^{(2)} = \frac{1}{4} \sqrt{\frac{5}{6\pi}} \; \eta \, V_{zz}$$

the x, y, and z-axes being the principal axes of the crystal. The asymmetry parameter is defined as

$$\eta = \frac{V_{xx} - V_{yy}}{V_{zz}} \quad \text{where} \quad |V_{zz}| \geq |V_{xx}| \geq |V_{yy}| \; . \tag{20}$$

Figure 3 shows a typical configuration for a particular crystal and propagation vectors of detected gammas, where we have taken the

z-axis of the crystal to coincide with the quantization axis - the z-axis of the coordinate system.

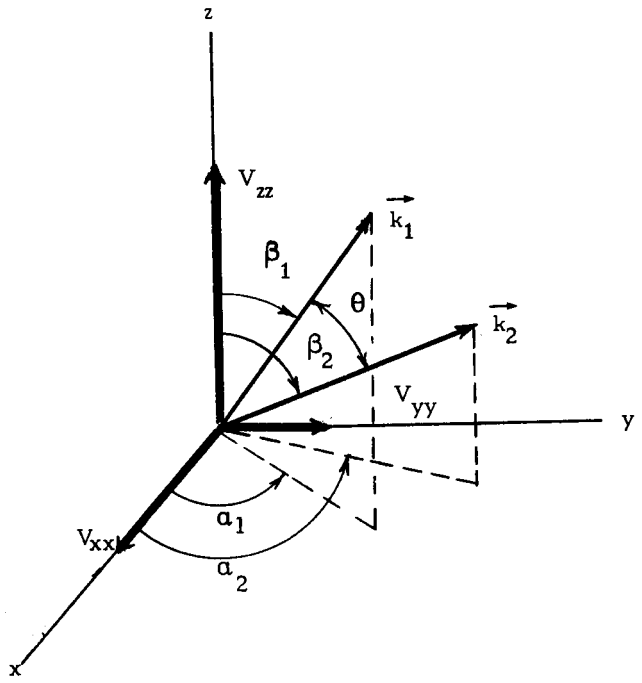

Figure 3. Arrangement of detected gamma radiations and crystalline field gradients for $\eta \neq 0$ case.

Conventionally, electric quadrupole moment is defined by (26, p. 525)

$$eQ = 4\sqrt{\frac{\pi}{5}}\ C(I\,2\,I;\ I,\ 0,\ I)\ \langle I \| T^{(2)} \| I \rangle$$

so equation (18) becomes

$$\langle I_m | \mathcal{H}_{el} | I_m' \rangle = \sqrt{\frac{\pi}{5}}\ (-)^q\ \frac{C(I\,2\,I;\ m, q, m')}{C(I\,2\,I;\ I,\ 0,\ I)}\ V^{(2)}_{-q}\ eQ\ .$$

Since $|q|$ can have values 0, 1, and 2, we get the following Hamiltonian matrix elements

$$H_{m,m} = \sqrt{\frac{\pi}{5}} \frac{C(I\,2\,I;\ m, 0, m)}{C(I\,2\,I;\ I, 0, I)} V_0^{(2)} eQ$$

$$H_{m,m\pm1} = \sqrt{\frac{\pi}{5}} (-)^{\pm1} \frac{C(I\,2\,I;\ m, \pm1, m\pm1)}{C(I\,2\,I;\ I, 0, I)} V_{\mp1}^{(2)} eQ \tag{21}$$

$$H_{m,m\pm2} = \sqrt{\frac{\pi}{5}} (-)^{\pm2} \frac{C(I\,2\,I;\ m, \pm2, m\pm2)}{C(I\,2\,I;\ I, 0, I)} V_{\mp2}^{(2)} eQ.$$

Evaluating the Clebsch-Gordon coefficients (10, p. 1009) and substituting in values of $V_q^{(2)}$ from equation (19)

$$H_{m,m} = \frac{3m^2 - I(I+1)}{I(2I-1)} \frac{eQ\,V_{zz}}{4}$$

$$H_{m,m\pm1} = 0 \tag{22}$$

$$H_{m,m\pm2} = \frac{\sqrt{(I\pm m+2)(I\pm m+1)(I\mp m)(I\mp m-1)}}{8I(2I-1)} eQ\,\eta V_{zz}.$$

For future reference, we define several important constants. Corresponding to the smallest non-vanishing energy difference for transitions between states

$$\omega_o = \frac{3eQ\,V_{zz}}{2I(2I-1)\hbar} \tag{23}$$

for the case of odd-half-integer spins and

$$\omega_o = \frac{3eQ\,V_{zz}}{4I(2I-1)\hbar} \tag{24}$$

for the case of even-half-integer spins. ω_o is equal to $\frac{2\pi}{T}$ where T is the quadrupole precession period.

The quadrupole frequency ω_E is defined by

$$\omega_E = \frac{eQ\,V_{zz}}{4I(2I-1)\hbar} \tag{25}$$

and is equal to $\frac{\omega_o}{6}$ for the case of odd half-integer spins and $\frac{\omega_o}{3}$ for even half-integer spins.

The quadrupole coupling $\Delta\nu_Q$ is often used to designate the strength of the quadrupole interaction, and is defined by

$$\Delta\nu_Q = \frac{eQ\,V_{zz}}{h}. \tag{26}$$

Also useful are the quantities $Q^* = \frac{\omega_o t}{\pi}$ and $x = \omega_E t$ where t is the interaction time - the time delay between emission of γ_1 and γ_2.

For the polycrystalline case, we average (6) over all orientations of a frame or reference attached to the crystal. This procedure is equivalent to keeping the frame of reference stationary and moving the detectors over the surface of a sphere while keeping the angle $(\vec{k}_1, \vec{k}_2)$ fixed. We will make three rotations of the coordinate system attached to the crystal in order to facilitate this calculation:

1. Rotation about the z-axis through the angle α_1.
2. Rotation about the new y-axis through angle β_1.
3. Rotation about the new z-axis through angle γ until $\vec{k}_1, \vec{k}_2$ and the final x-axis are coplanar.

These three rotations are illustrated in Figure 4.

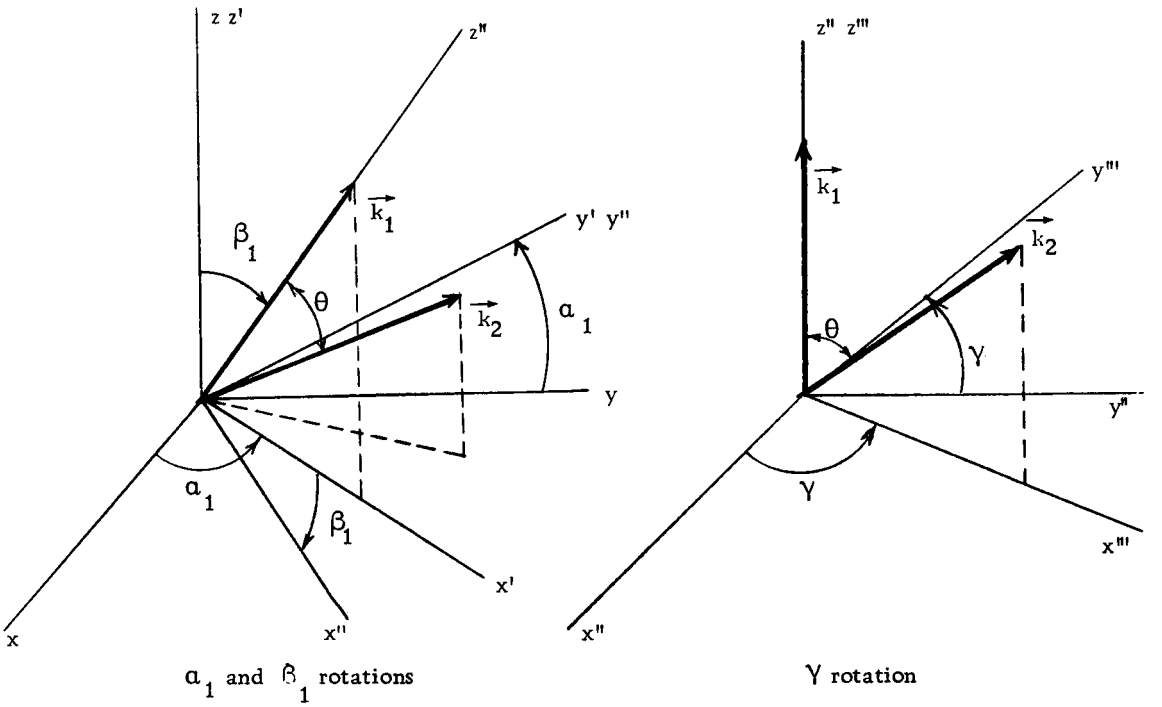

Figure 4. Rotation of coordinate system of a crystal through Euler angles α_1 β_1 and γ.

Applying the rotation matrix elements to the spherical harmonics, we obtain for the average over all orientations

$$\overline{W(\vec{k}_1, \vec{k}_2; t)} = \frac{1}{8\pi^2} \sum_{n, n'} \sum_{\nu_1, \nu_2} \sum_{s_1, s_2} (-)^{2s_2} G^{s_1 s_2}_{\nu_1 \nu_2}(t) \frac{4\pi}{[(2\nu_1+1)(2\nu_2+1)]^{\frac{1}{2}}}$$

$$\times B\nu_1(\gamma_1) B\nu_2(\gamma_2) \int_{\alpha=0}^{2\pi} \int_{\beta=0}^{\pi} \int_{\gamma=0}^{2\pi} D^{\nu_1}_{n, s_1}(\gamma \beta_1 \alpha_1) Y^{n}_{\nu_1}(0, 0)$$

$$\times D^{*\nu_2}_{n', s_1}(\gamma \beta_1 \alpha_1) Y^{*n'}_{\nu_2}(\theta, 0)\, d\alpha_1 d\cos\beta_1 d\gamma. \qquad (27)$$

Using the orthonormality property of rotation matrices (29, p. 75),

and evaluating the spherical harmonics, we obtain the probability function for the case of an electric quadrupole interaction in a polycrystalline source as

$$\overline{W(\vec{k}_1, \vec{k}_2; t)} = \sum_{\nu_1 \nu_2} \sum_{s_1 s_2} (-)^{2s_2} G^{s_1 s_2}_{\nu_1 \nu_2}(t) \frac{P_{\nu_2}(\cos\theta)}{[(2\nu_1+1)(2\nu_2+1)]^{\frac{1}{2}}} B_{\nu_1}(\gamma_1) B_{\nu_2}(\gamma_2)$$

$$\times \delta_{s_1 s_2} \delta_{\nu_1 \nu_2}. \tag{28}$$

Axially Symmetric Case

If the electric field gradient has axial symmetry, $\eta = 0$, the Hamiltonian matrix is diagonal, and the elements of the unitary matrix in equation (14) are

$$\langle I_b m_z | U | I_b m_b'' \rangle^* \langle I_b m_z | U | I_b m_b \rangle = \delta_{m_z m_b} \delta_{m_z m_b''}$$

$$\langle I_b m_z' | U | I_b m_b''' \rangle \langle I_b m_z' | U | I_b m_b' \rangle^* = \delta_{m_z' m_b'''} \delta_{m_z' m_b'}.$$

Letting $s_1 = s_2 = s$ and $\nu_1 = \nu_2 = \nu$ and substituting (14) into (28) we obtain for this case

$$\overline{W(\vec{k}_1, \vec{k}_2; t)} = \sum_{\nu} \sum_{m_z, m_z'} [C(I_b I_b \nu; m_z, -m_z', s)]^2$$

$$\times \left[\cos\left(\frac{E_{m_z} - E_{m_z'}}{\hbar} t \right) - i \sin\left(\frac{E_{m_z} - E_{m_z'}}{\hbar} t \right) \right] \frac{P_\nu(\cos\theta)}{2\nu+1}$$

$$\times B_\nu(\gamma_1) B_\nu(\gamma_2) \tag{29}$$

where the sum over s is dropped since $s = m_z - m_z'$.

From (22) we notice that $E_{m_z} = E_{-m_z}$. This relation plus the fact that $[C(I_b I_b \nu;\ m_z, -m_z', s)]^2 = [C(I_b I_b \nu;\ m_z', -m_z, s)]^2$ leads to disappearance of the sine term in (29), so that $\overline{W(\vec{k}_1, \vec{k}_2; t)}$ is entirely real. Comparing equation (29) with equation (8), we find that perturbation factors for the axially symmetric electric quadrupole interaction are

$$G_\nu(t) = \frac{1}{2\nu+1} \sum_{m_z m_z'} [C(I_b I_b \nu;\ m_z, -m_z', s)]^2 \cos\left(\frac{E_{m_z} - E_{m_z'}}{\hbar} t\right). \quad (30)$$

Non-Axially Symmetric Case

With no restrictions on the symmetry of the perturbing static field, the interaction Hamiltonian H_Q, equation (22), now contains off-diagonal elements and must be diagonalized in order to find the eigenvalues E_{m_z} and elements of the unitary matrix, U. Combining equations (28) and (14) we find

$$\overline{W(\vec{k}_1, \vec{k}_2; t)} = \sum_{\nu_1, \nu_2} \sum_{s_1, s_2} (-)^{2s_2} \sum_{m_z, m_z'} \sum_{m_b, m_b''} (-)^{m_b' + m_b'' - 2I_b}$$

$$\times\ C(I_b I_b \nu_1;\ m_b, -m_b', s_1)\ C(I_b I_b \nu_2;\ m_b'', -m_b''', s_2) \langle I_b m_z | U | I_b m_b'' \rangle^*$$

$$\times\ \langle I_b m_z | U | I_b m_b \rangle \langle I_b m_z' | U | I_b m_b''' \rangle \langle I_b m_z' | U | I_b m_b' \rangle^*$$

$$\times\ e^{-i/\hbar (E_{m_z} - E_{m_z'}) t} \frac{P_{\nu_2}(\cos\theta)}{[(2\nu_1+1)(2\nu_2+1)]^{\frac{1}{2}}} B_{\nu_1}(\gamma_1) B_{\nu_2}(\gamma_2)\, \delta_{s_1 s_2} \delta_{\nu_1 \nu_2}$$

and setting $s_1 = s_2 = s$ and $\nu_1 = \nu_2 = \nu$ we get

$$\overline{W(\vec{k}_1, \vec{k}_2; t)} = \sum_{\nu} \sum_{s} \sum_{m_z, m_z'} \sum_{m_b, m_b''} C(I_b I_b \nu; m_b, -m_b', s)$$

$$\times\ C(I_b I_b \nu; m_b'', -m_b''', s) \langle I_b m_z | U | I_b m_b'' \rangle^* \langle I_b m_z | U | I_b m_b \rangle$$

$$\times\ \langle I_b m_z' | U | I_b m_b''' \rangle \langle I_b m_z' | U | I_b m_b' \rangle^* e^{-i/\hbar (E_{m_z} - E_{m_z'}) t}$$

$$\times\ \frac{P_\nu(\cos\theta)}{2\nu + 1} B_\nu(\gamma_1) B_\nu(\gamma_2) . \tag{31}$$

Comparing equation (31) with equation (8) we get the perturbation factors for the electric quadrupole interaction to be

$$G_\nu(t) = \sum_{s} \sum_{m_z, m_z'} \sum_{m_b, m_b''} \frac{1}{2\nu+1} C(I_b I_b \nu; m_b, -m_b', s)$$

$$\times\ C(I_b I_b \nu; m_b'', -m_b''', s) \langle I_b m_z | U | I_b m_b'' \rangle^* \langle I_b m_z | U | I_b m_b \rangle$$

$$\times\ \langle I_b m_z' | U | I_b m_b''' \rangle \langle I_b m_z' | U | I_b m_b' \rangle^* e^{-i/\hbar (E_{m_z} - E_{m_z'}) t} . \tag{32}$$

Apparatus

Description of Coincidence Spectrometer

Data for this experiment was taken using a delayed coincidence spectrometer. The spectrometer used is the same as that used and described by Sommerfeldt (34) except for changes in the

photomultiplier tubes and associated circuitry to be described later. A block diagram is shown in Figure 5 for reference.

The delayed coincidence spectrometer is used to study the time and spatial relations between two radiations emitted in a nuclear deexcitation cascade. The spectrometer must select the genetically related radiations of interest, measure the angle between propagation vectors of these radiations, and measure the time lapse between emission of them.

Gamma radiations are detected by using standard $1'' \times 1\frac{1}{2}''$ NaI(Tl) scintillation crystals which are optically coupled to Amperex 56 AVP photomultiplier tubes. The angle between propagation vectors of the radiations is determined by the angle between the axes of the detecting crystals.

The spectrometer may be logically separated into fast and slow functions. These two functions are separated at the photomultiplier tube. Pulses from the anode are used to drive a Western Electric 404A vacuum tube limiter to cutoff. The limited pulses, after being delay line clipped to length T = 200 nanoseconds, are fed into a time-to-amplitude converter (TAC). This converter is essentially a fast coincidence circuit which produces output pulses which are proportional in amplitude to the overlap time of the two limited fast pulses. After being delay line shaped, the TAC output pulses are pulse height analyzed by a gated 512 channel analyzer.

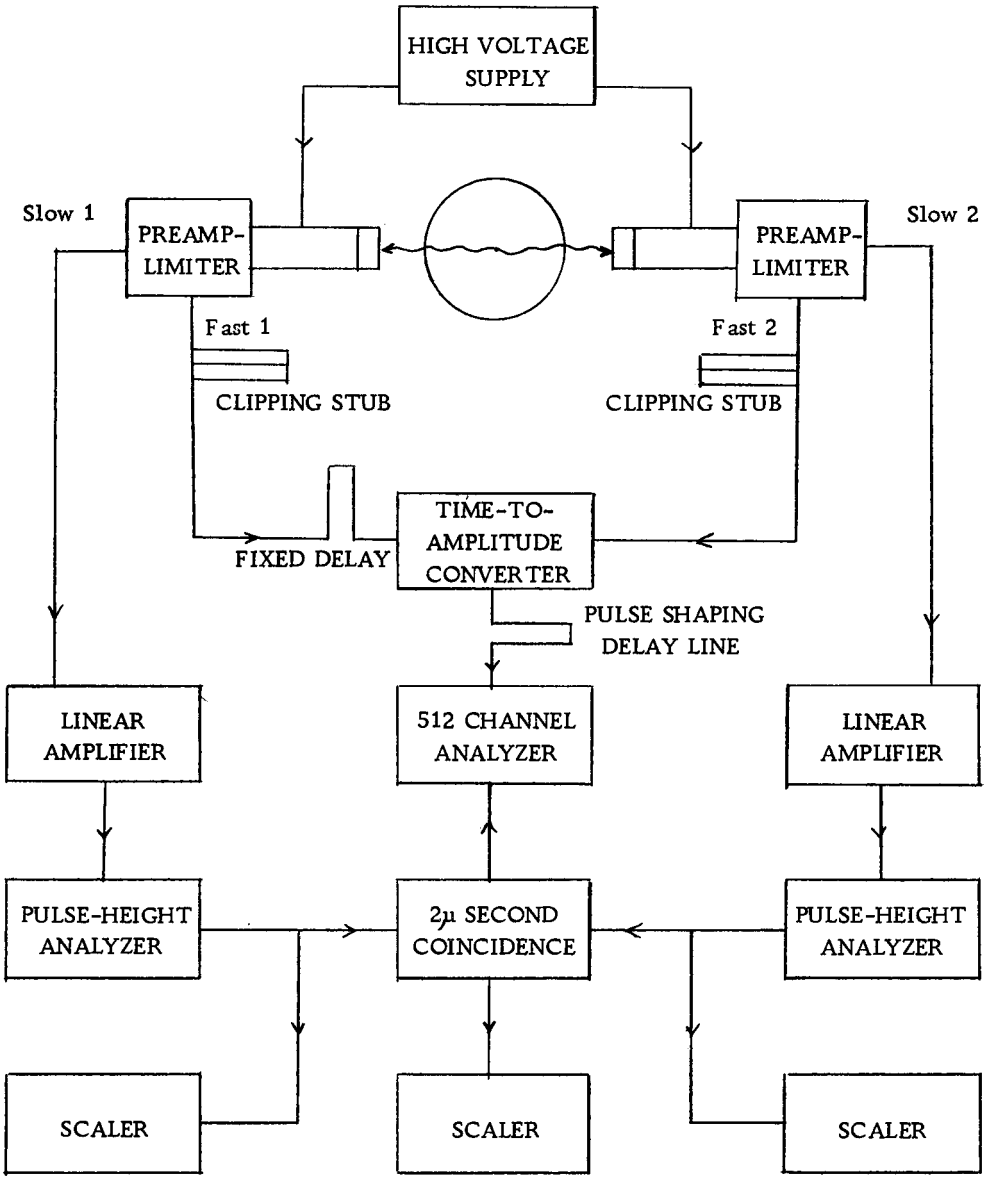

Figure 5. Block diagram of delayed coincidence spectrometer.

Since the TAC will produce an output pulse for all radiations occuring within 2T of each other, some means must be provided for preventing analysis of all but those corresponding to genetically related events of the proper energies. The slow circuitry provides this function. Slow pulses are taken from the ninth dynode of the 56AVP. Following amplification, the slow pulses in each channel enter a single channel analyzer which is set to select only gamma radiations of desired energy. The single channel output pulses are fed into a two-microsecond slow coincidence circuit which produces output pulses when radiations of the selected energies occur within the resolving time of this circuit. These coincidence output pulses are used to gate the 512 channel analyzer, assuring that the TAC pulses analyzed correspond to the desired cascade. Because input pulses are proportional to the time lapse between gamma radiations, the output of the analyzer can, when time calibrated, be read as number of coincidence counts vs. time.

Development Work on Coincidence Spectrometer

As mentioned previously, one of the purposes of the coincidence spectrometer is to measure the time delay between two genetically related gamma radiations. The response of the system to two gamma radiations being emitted from the nucleus simultaneously (prompt cascade) has a finite width. Schwarzschild (31, p. 30) attributes

this largely to four causes:

1. Variation of time of interaction of the radiation with the scintillator.

2. Finite decay time of the light emitting states in the phosphor and variation of photon flight to the multiplier cathode.

3. Variation of transit time of photoelectrons and secondary emission electrons in the photomultiplier due to (a) different path lengths (b) variation of initial energy and angle of secondary electrons.

4. Jitter and uncertainties of time of triggering of associated electronics.

Measurement of the width of the prompt function at one half of its maximum value ($2\tau_{\frac{1}{2}}$) is generally used as a figure of merit for time resolution. It is desirable to have the prompt response function be narrow in order to see as much detail as possible in the delayed coincidence spectrum. It was felt that some improvement in time resolution over that of previous experiments could be gained in area 4 by using solid state or nuvistor circuitry in place of vacuum tubes in the limiter and TAC circuits and in area 3 by replacing the RCA 6810A photomultiplier tubes with Amperex 56AVP tubes.

Two limiter circuits were tried, one using Amperex PADT 51 avalanche transistors and the other using RCA 7895 nuvistors. No successful method of achieving good clipping was found for the PADT 51 circuits. The 7895 limiters showed no improvement in

prompt resolution over the previously used 404A circuits. Furthermore, it was necessary to use two 7895's in parallel in order to obtain limited pulses of amplitude comparable with those obtained from a single 404A.

A time-to-amplitude converter consisting of a diode discriminator and 2N501A transistor integrator circuit was developed which has stability, resolution, and sensitivity comparable to the Green and Bell 6BN6 circuit presently used. This circuit seemed to offer no advantage in resolution over the 6BN6 circuit, so was not used.

The 6810A photomultiplier tubes were replaced by Amperex 56AVP tubes which reputedly have more uniform electron time-of-flight characteristics from photocathode to first dynode and should offer some improvement in resolution. It was found that these tubes were considerably noisier than the 6810A's working at approximately the same inter-dynode voltages. Although the noise pulses are very small compared to nuclear pulses, they are sufficiently large to appear at the limiter output and adversely affect the prompt curve if the tube voltages are sufficiently high. Considerable time was devoted to changing voltage dividers, anode load resistors, and applied voltages in order to optimize the prompt response function. A voltage divider designed for high gain (type A), a divider designed for high output current (type B), as well as a compromise between the two were tried with no apparent differences in resolution. The

compromise circuit was finally settled upon, and an optimum $2\tau_{\frac{1}{2}}$ of 3.31 nanoseconds (as compared with $2\tau_{\frac{1}{2}}$ of 3.85 nanoseconds for the 6810A tubes) was achieved using positron annihilations and gating the single channel analyzers at 133 and 482 kilovolts. The vacuum tube distribution system previously used for the photomultiplier tubes was replaced with standard voltage dividers, both 56AVP's being driven by a single high voltage supply. This change seemed to have no effect on stability or resolution.

This development study brought out the fact that, as pointed out by Schwartzschild, most of the time jitter is due to scintillator decay time and photomultiplier jitter. Replacing the photomultiplier anode pulses with those from a mechanical pulse generator, a $2\tau_{\frac{1}{2}}$ of 0.285 nanosecond was obtained as a measure of the instrumental resolution for all of the circuitry except the photomultiplier and scintillator. A $2\tau_{\frac{1}{2}}$ of 0.420 nanosecond was obtained by placing a nanosecond light pulser between the two 56AVP s and observing the prompt curve.

Bell (5) has shown that the standard deviation for arrival of the n-th photoelectron at the photomultiplier anode should be

$$\sigma_n = \sqrt{\frac{\sigma^2}{n} + n(\tau_p/R)}$$

where σ = the time uncertainty in arrival of the multiplicative cascade at the photomultiplier output, assumed here to be the standard

deviation of a Gaussian distribution, τ_p = decay constant of the phosphor, and R = total photoelectrons produced at the photocathode.

For a prompt resolution of Gaussian shape, the full width at half maximum is given by

$$2\tau_{\frac{1}{2}} = 2\sigma_n \sqrt{2/3 \ln 2} = 1.92\sigma_n$$

where the circuit responds to the average time of arrival of the first n photoelectrons. For NaI (Tl) scintillators $\tau_p \approx 250$ nanoseconds, $R \approx 2000$ electrons for 510 kilovolt gammas, and $\sigma \approx 1$ nanosecond. If we assume that the circuit responds to an average of eight photoelectrons then $\sigma_n = 1.06$ nanosecond and $2\tau_{\frac{1}{2}} \approx 2$ nanoseconds.

A $2\tau_{\frac{1}{2}} = 1.84$ nanosecond was measured on the 56AVP spectrometer for 512-512 kilovolt annihilation radiation. Apparently significant improvements in time resolution await improvements in time response of radiation detectors.

Experimental Measurements

An experiment to determine anisotropy vs. time for Hf^{181} embedded in a polycrystalline source of hafnium metal was performed using the 56AVP spectrometer. The energy levels and decay scheme of Hf^{181} are shown in Figure 6. The experiment was performed to determine the effect of perturbations on the 10-nanosecond excited level. Delayed coincidence measurements were made on the 133-482

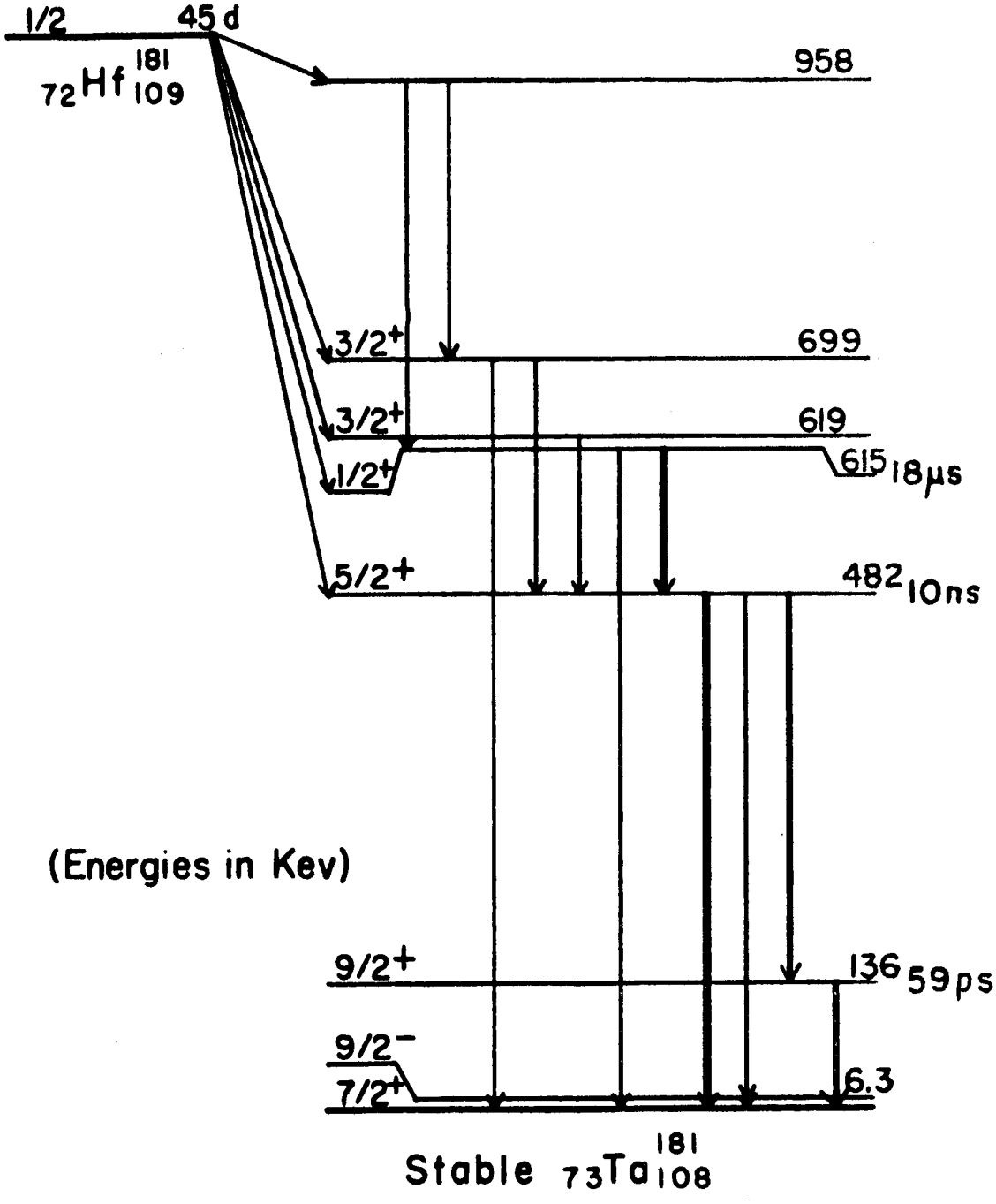

Figure 6. Energy levels and decay scheme for hafnium-181.

kilovolt cascade. To select these energies from among those of the other radiations present, the single channel analyzers were set to straddle appropriate energy peaks, as described by Sommerfeldt (34).

The calibration procedure, method of correction for chance counts, and normalization to the product of singles counts were the same as those used and described by Sommerfeldt. Data for these experiments were taken alternately at 90° and 180° every two hours. Several time calibrations were made during each experiment, and in no case was it found necessary to correct for changes in the calibration of 1.03 nanoseconds per channel. Data for those channels containing the steep leading edge were normalized to the total coincidence count and plotted for each experiment. The location of this edge is very sensitive to drift of the position of the time spectrum. For no run was the leading edge drift found to be more than one-half channel.

Hf^{181} was obtained by neutron irradiation of pure hafnium metal in a Hanford reactor. The sample was graded to be composed of microcrystals of under 53 microns in diameter.

A counting source was made up of approximately 10 milligrams of the irradiated metal. This material was placed in a 3/16-inch high by 1/8-inch diameter (approximately) thin-walled fluorethelyne capsule. Three experiments were performed as follows:

1. Description: The source capsule was placed in a fluorethelyne source holder duplicating geometry of the previously performed experiments with 6810A photomultiplier tubes.

   Length of experiment: 27 hours running time at each (180° and 90°) angle.

   Purpose: To compare performance of the 56AVP spectrometer with the 6810A spectrometer.

   Conclusion: Anisotropy vs. time data duplicates that obtained with old spectrometer within statistical errors.

2. Description: The source capsule was placed between the pole pieces taken from the magnetron magnet to be used in the mixed case experiment.

   Length of experiment: 30 hours running time at each angle.

   Purpose: To determine effects of scattering due to the pole pieces.

   Conclusion: No apparent scattering effects were observed.

3. Description: Repeated experiment 1 following 72-hour experiment with source in eight-kilogauss field.

   Time: 24 hours running time at each angle.

   Purpose: To determine if there is any polarization of the source due to an applied magnetic field.

   Conclusion: No polarizing effects were observed.

Since no indication of scattering or polarization were evident, data from these three experiments were combined, corrected for accidentals, and normalized to the product of the singles for comparison with theoretical calculations. For the three experiments, totals of about 80,000 counts were accumulated in the highest count

channels. The true-to-chance ratio for these experiments was approximately 80:1 in the peak channels.

Results and Conclusions

Because of the apparent periodic behavior of the results, they were analyzed in terms of the theory for the axially symmetric electric quadrupole interaction. Calculations of anisotropy $A(t) = \frac{W(\pi, t)}{W(\pi/2, t)} - 1$ were made based on this theory with corrections for the solid angle subtended by the detectors. The prompt time response of the spectrometer was accounted for by calculating the convolution integral

$$\overline{W(\theta, t)} = \int W(\theta, T)\ \rho(T-t)\, dT$$

where $\rho(T-t)$ is the prompt response function of the spectrometer and $W(\theta, t)$ is the solid angle corrected probability function. Comparison of the periodicity of these calculations with experimental results (Figure 7) indicates a precession period of 21.0 ± 0.5 nanoseconds, corresponding to an interaction strength $\omega_0 = 299 \pm 8$ Mc./Sec.

Divergence of the theory from experimental results may most likely be attributed to two causes: (1) lack of axial symmetry in the electric field gradient, and (2) variation in magnitude of the gradient from nucleus to nucleus. These possibilities may be due to imperfections in the crystal or nuclear recoil effects. In order to obtain

some quantitative estimate of each of these causes, further calculations were made based on the theory for the electric quadrupole interaction with a non-axially symmetric field gradient. Calculations were made using values of the asymmetry parameter η between 0.25 and 0.40 in increments of 0.05, the best fit being obtained at $\eta = 0.30$ as shown in Figure 8.

Values of $G_\nu(t)$ used in calculating $W(\theta, t)$ were obtained from W. Schneider of Uppsala, Sweden. These functions were calculated by him from equation (32) by means of an electronic computer. The eigenvalues and elements of the unitary matrix were computed by diagonalization of a six-by-six Hamiltonian matrix for each of 141 values of the parameter Q^* in increments of $\Delta Q^* = 0.050$. The diagonalization was performed by using the modified Jacobi method of numerical diagonalization (15).

Figure 9 represents a further improvement in the fit made from calculations containing solid angle corrections and the response function of the spectrometer, as well as a distribution of interaction frequencies as suggested by Matthias et al.(24). Calculations were made for the frequency smeared perturbation coefficients $\overline{G_\nu(t)}$ by means of the integral

$$\overline{G_\nu(t)} = \frac{\int G_\nu(\omega_E t)\, P(\omega_E - \omega_E^{o})\, d\omega_E}{\int P(\omega_E - \omega_E^{o})\, d\omega_E}$$

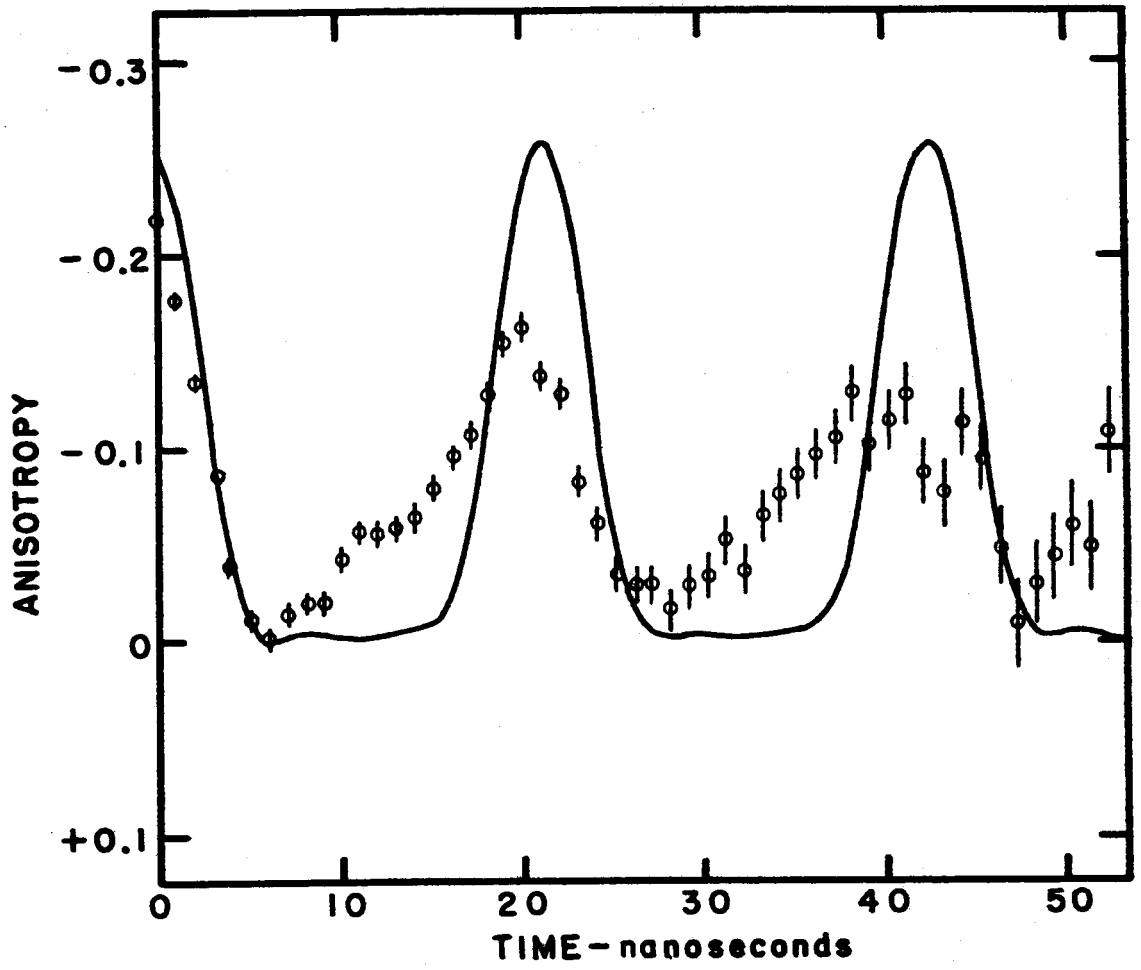

Figure 7. The anisotropy of the 133-482 kilovolt gamma-gamma cascade obtained with a polycrystalline source. The solid curve is calculated from the theory assuming a static interaction with an axially symmetric electric-field gradient.

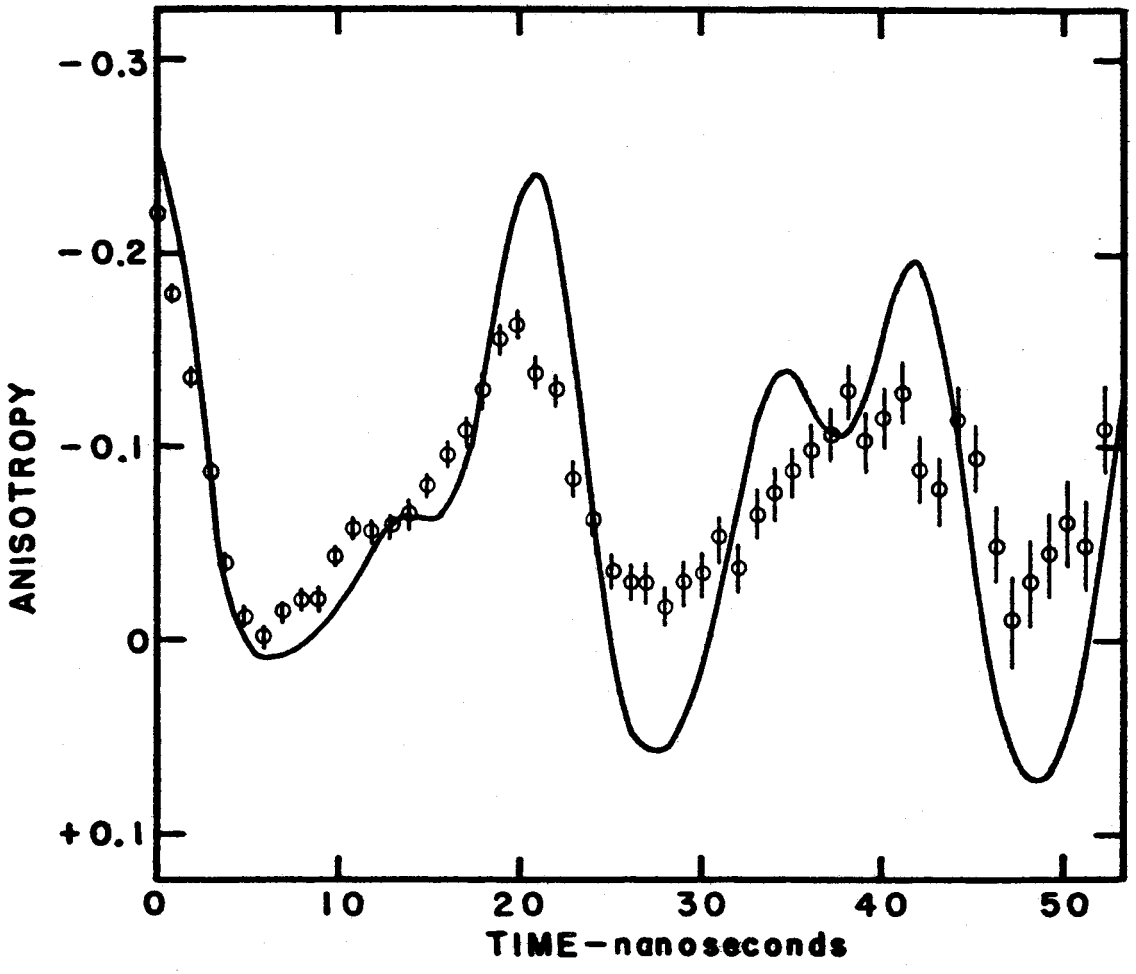

Figure 8. Comparison of the measured anisotropy with a rhombic interaction using an asymmetry parameter $\eta = 0.30$.

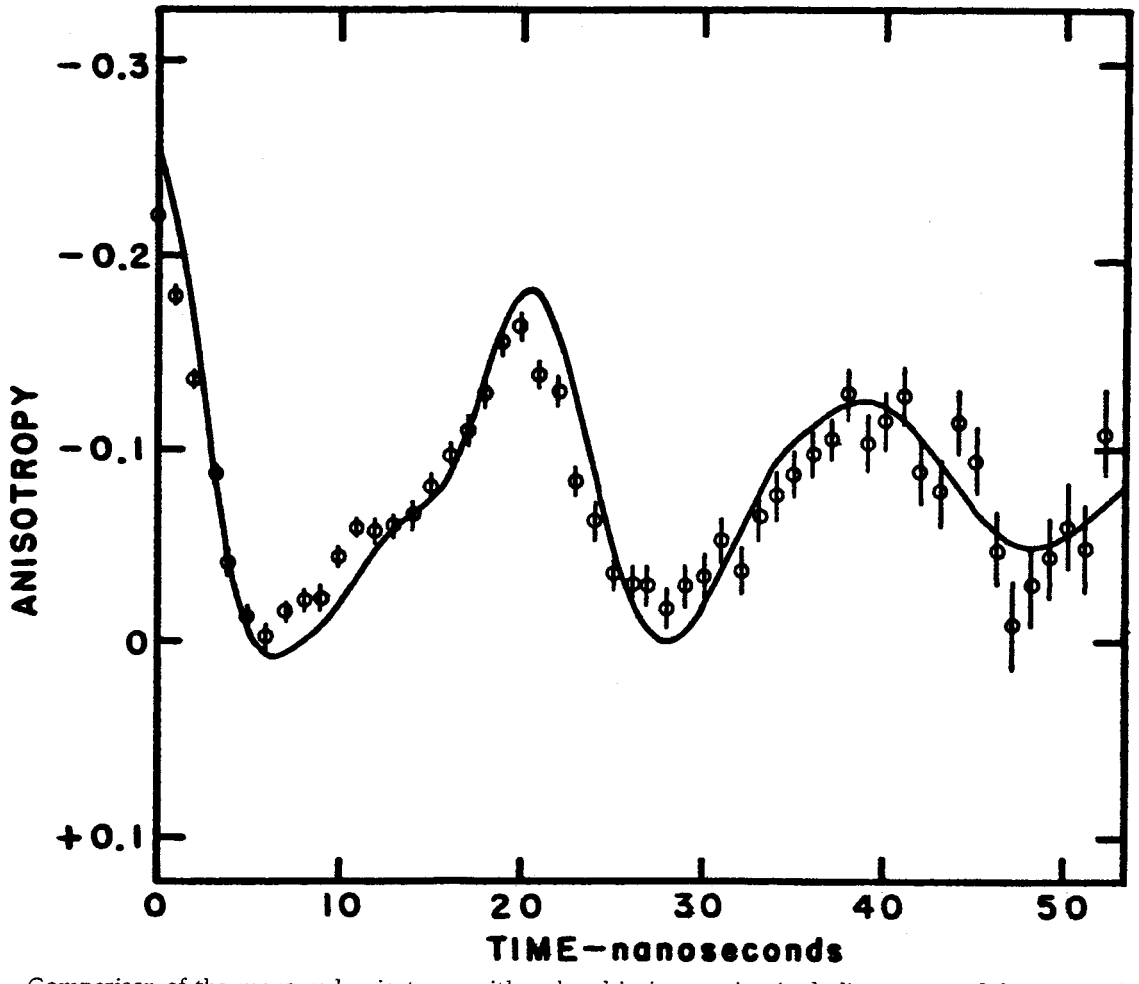

Figure 9. Comparison of the measured anisotropy with a rhombic interaction including a normal frequency distribution having a full width at half-maximum of 10%.

using a Gaussian

$$P(\omega_E - \omega_E^o)\, d\omega_E = \frac{1}{\sigma\sqrt{2\pi}}\, e^{-[(\omega_E - \omega_E^o)^2/2\sigma^2]}\, d\omega_E$$

as an estimate of the distribution in the electric field gradient, where ω_E^o is the centroid and $\delta = \frac{\sigma}{\omega_E^o}$ the relative width of the function. Values of δ = 5%, 10%, and 15% were assumed. For each δ, the same values of η were used as in the calculation without the frequency distribution. Figure 9 represents the best fit which was obtained with $\eta = 0.30$ and $\delta = 10\%$.

Since ω_o has been measured experimentally, one might hope to calculate Q from equation (23). A value of Q determined in this way would be useful as a test of nuclear models. Unfortunately, the quadrupole moment cannot be determined directly from perturbed angular correlations since it always appears as a coefficient of V_{zz}. The field gradient in crystals is not very accurately known, and estimates of it allow one to calculate only very approximate values of Q.

On the other hand, one can use ω_o to estimate the electric field gradient from a model dependent calculation of Q. The collective nuclear model is applicable to nuclei having many nucleons outside of a closed shell. Such nuclei are greatly deformed since the outer nucleons act coherently to deform the core into a spheroidal shape. Ta^{181} is an example of an isotope possessing such a nucleus.

Nuclei of this type exhibit many relatively low lying energy levels which are quantum mechanical rotation and vibration states. These levels are easily excited by passing charged particles near the nucleus, the so-called coulomb excitation process. It is possible to calculate Q for the nucleus from the collective model using either coulomb excitation cross sections or gamma decay transition rates.

From perturbation theory it can be shown that the total cross section for coulomb excitation of order λ is (4)

$$\sigma_{E\lambda} = \left(\frac{mZ_i e}{\hbar^2 k_i}\right)^2 a^{-2\lambda+2} B(E\lambda)\, f_{E\lambda}(\xi) \tag{33}$$

where m is the reduced mass of the nucleus and projectile and a is half of the distance of approach for a head-on collision and is given by

$$a = \frac{mZ_i Ze^2}{\hbar^2 k_i k_f} \approx \frac{Z_i Z e^2}{\hbar k v}$$

and ξ is a dimensionless parameter given by

$$\xi = \frac{mZ_i Z e^2}{\hbar^2}\left(\frac{1}{k_f} - \frac{1}{k_i}\right) \approx \frac{mZ_i Z e^2}{\hbar^2 k}\,\frac{\Delta E}{2E}\,.$$

$B(E\lambda)$ is the reduced matrix element for the transition from initial states of momentum k_i to final states of momentum k_f. The approximations hold for the semiclassical case where k is an average

over slightly different k_i and k_f and E and ΔE are the ion and excitation energies, respectively. Values of $f_{E\lambda}(\xi)$ have been tabulated by Alder et al. (4, p. 458). Alder has shown that the reduced transition matrix for decay is related to that for excitation by

$$B(\lambda\ ;\ I_f \rightarrow I_i) = \frac{2I_i + 1}{2I_f + 1}\ B(\lambda\ ;\ I_i \rightarrow I_f)\ . \tag{34}$$

The intrinsic quadrupole moment is related to the reduced transition matrix by

$$B(E2;\ I_i \rightarrow I_f) = \frac{5}{16\pi}\ e^2 Q_o^2\ C(I_i 2 I_f\ ;\ K\ O\ K) \tag{35}$$

where K is the spin of the nucleons within the nucleus. Derivation of this formula is based on the fact that the intrinsic structure of the nucleus is unaltered by rotational transitions. The transition matrix element can be expressed in the form of the intrinsic quadrupole moment Q_o multiplied by a vector addition coefficient.

Using protons, Stelson and McGowan (25) have done coulomb excitation studies of Ta^{181} to determine B(E2) from excitations to the 303 kilovolt level. Their results, averaged over a number of proton energies, give $B(E2)_{ex} = 5.45 \pm 0.44$ barns^2. The 303-kilovolt to ground level transition takes place between spins 11/2 and 7/2, so using equation (34) we get

$B(\lambda\ ;\ I_f \rightarrow I_i) = B(2;\ 11/2 \rightarrow 7/2) = (3.63 \pm 0.29) \times 10^{-1}$ barn^2 and from equation (35) one finds $eQ_o = 7.083$ barns.

The intrinsic quadrupole moment Q_o measures the eccentricity of charge distribution as seen in the body-fixed system, which is rotating with respect to the laboratory system. The charge distribution in the laboratory is thus smeared out with respect to that observed in the body-fixed system. This smearing effect is accounted for by multiplying Q_o by a coefficient derived on the basis of quantum mechanical wave functions which describe the rotation. The resultant observed quadrupole moment is

$$eQ = \frac{3K^2 - I(I+1)}{(2I+3)(I+1)} \, eQ_o \tag{36}$$

for the level of spin I.

We wish to calculate eQ for the 482-kilovolt level which has $I = 5/2$. This spin value, together with the inhibited E2 transition for this state to the ground and 136-kilovolt states, indicate a different particle configuration from that of the ground state. If roughly the same particle configuration is assumed, the Mottelson and Nilsson (27) classification predicts that the next rotational band will have $K = 5/2$. Substituting these values for I and K into equation (36), we obtain

$$eQ = (2.53 \pm 0.10) \text{ barns}.$$

Using our interaction strength of $\omega_o = 299 \pm 8$ Mc./Sec. and $\eta = 0.30$ one finds from equation (20) and the Laplace equation, $\nabla^2 V = 0$, that

$$V_{zz} = \pm (5.18 \pm 0.27) \times 10^{17} \text{ volts/cm.}^2$$

$$V_{yy} = \mp (3.37 \pm 0.19) \times 10^{17} \text{ volts/cm.}^2$$

$$V_{xx} = \mp (1.81 \pm 0.25) \times 10^{17} \text{ volts/cm.}^2$$

are the components of the electric field gradient in hafnium metal. From equation (26) one calculates the quadrupole coupling to be $\Delta\nu_Q = 317$ Mc./Sec.

In principle, one should be able to use the quadrupole coupling to calculate the quadrupole moment if the electric field gradient is known. T. P. Das[1] has suggested using a method described by himself and Pomerantz (11) for calculating the field gradient due to ions in the hexagonal close packed lattice sites. The paper is based on a calculation of the ionic field gradient $q_{lattice} = \sum_i (3 z_i^2 - r_i^2)/r_i^5$ using the method of Nijboer and DeWette. For the hafnium close packed structure $a = 3.1952$ Å and $c = 5.0569$ Å giving a c/a ratio of 1.583. From Figure 1 of the Das and Pomerantz paper one finds the electric field gradient to be $0.20/a^3$ cm.$^{-3}$ per unit ionic charge. Assuming the ions making up the lattice are Hf++, then if the Ta^{181} nuclei are in substitutional Hf sites, and are not surrounded by core electrons, they would experience a field gradient of $2 \times 0.2\, e/a^3$ cm.$^{-3}$.

Because of the presence of an electric field in the region of the core electrons, a quadrupole moment is induced in the core

[1] Private communication.

electron structure. This shell distortion alters the field gradient at the lattice sites. The amount by which this field is altered is accounted for by the factor $(1 - \gamma_\infty)$ where γ_∞ is the Sternheimer antishielding factor discussed by Wikner and Das (39). By analogy with available anti-shielding factors in other ions, Das estimates $(1 - \gamma_\infty)$ to be 75 for the Hf++ case. Using this estimate, one obtains $q = 0.9 \times 10^{24}$ cm.$^{-3}$. In units which allow comparison with V_{zz} calculated on page 41 we have

$$V_{zz} = \frac{1}{4\pi\epsilon_o} eq = 1.30 \times 10^{17} \text{ volts/cm.}^2$$

corresponding to a quadrupole coupling of $\Delta\nu_Q = 79.2$ Mc./Sec.

Das and Pomerantz (11) have made calculations of V_{zz} based on experimentally determined $\Delta\nu_Q$ values for several different metals. Their results indicate that the ionic contribution to the field gradient is usually about 30%, while the remainder is due to conduction electrons. If we assume that the difference in gradients is indeed due to conduction electrons, comparing the results on this page with those on page 41 one finds a 25% ionic contribution with the remaining 75% being due to conduction electrons.

Because of recoil during formation and decay of Hf^{181}, many of the Ta^{181} are probably situated in interstitial sites, and so calculations based on the field gradient at lattice sites may only be of value in estimating the order of magnitude of the field gradient.

As yet, no method has been devised for calculating field gradients due to conduction electrons, either at lattice sites or institials. Calculation of gradients at interstitials is a very complex problem, since the presence of an ion at an interstitial site not only distorts the lattice around the interstitial, but also affects the electron density around the interstitial. It appears that considerable work remains to be done in order to get a very satisfactory description of the internal fields in metals.

PERTURBED DIRECTIONAL CORRELATION WITH COMBINED MAGNETIC DIPOLE AND NON-AXIALLY SYMMETRIC ELECTRIC QUADRUPOLE INTERACTION

Theory

Introduction

The theory for the mixed interaction including asymmetry of the electric field gradient has been developed for specific cases by several authors. Pound (28) was first to discuss this case for the high magnetic field case in a paper describing the effects of electric quadrupole interactions on nuclear magnetic resonance absorption in solids. Dean (12) and Cohen (8) have treated the first-order Zeeman effect (low field) on nuclear quadrupole splitting for half-integer spin values. Lamarche and Volkoff (19) have calculated nuclear energy levels for any value of the ratio of electric quadrupole to magnetic dipole interaction and the special case of $I = 5/2$, asymmetry parameter $\eta = 0.95$ with the H field parallel to the principal z-axis of the electric field gradient. The general theory covering all values of asymmetry and y, as well as all possible relative orientations of the principal axes with respect to the direction of the magnetic field, has been developed by Matthias, Olsen, Schneider, and Steffen (21, 23). Their theory will be developed here in the notation of Rose (29).

The Magnetic Dipole Interaction

For the present case, we need to know the matrix elements of the magnetic dipole interaction Hamiltonian. This Hamiltonian is given by

$$\mathcal{H}_{magn} = -\vec{\mu} \cdot \vec{H} = -\mu_z H_o \tag{37}$$

$\vec{\mu} = \gamma \vec{I}$ being the magnetic dipole moment operator. The energy matrix elements are

$$< Im' | \mathcal{H}_{magn} | Im > = -H_o < Im' | \mu_z | Im >. \tag{38}$$

The energy matrix is diagonal since $\mu_z = \gamma I_z$, so we may write

$$< Im' | \mathcal{H}_{magn} | Im > = -H_o < Im | \mu_z | Im >. \tag{39}$$

Using the Wigner-Eckart theorem (29, p. 85)

$$< Im' | \mathcal{H}_{magn} | Im > = -H_o C(I\,1\,I;\, m, 0, m) < I \,||\vec{\mu}||\, I >. \tag{40}$$

Magnetic moment is defined (26, p. 524) by

$$\mu = < II | \mu_z | II > = C(I\,1\,I;\; I, 0, I) < I \,||\vec{\mu}||\, I >. \tag{41}$$

Substituting (40) into (41)

$$< Im' | \mathcal{H}_{magn} | Im > = -H_o \frac{C(I\,1\,I;\, m, 0, m)}{C(I\,1\,I;\, I, 0, I)} \mu. \tag{42}$$

Evaluating the Clebsch-Gordan coefficients, we obtain

$$< Im' | \mathcal{H}_{magn} | Im > = -H_o \mu \frac{m}{I} . \tag{43}$$

Defining the dipole interaction frequency

$$\omega_H = \frac{\mu H_o}{I\hbar} = \frac{\mu_N g H_o}{\hbar} \tag{44}$$

and the nuclear g-factor

$$g = \frac{\mu}{I \mu_N} \tag{45}$$

where μ_N = the nuclear magneton, we get for the final result,

$$< Im' | \mathcal{H}_{magn} | Im > = -\omega_H \hbar m \, \delta_{mm'} . \tag{46}$$

<u>The Combined Magnetic Dipole and Non-axially Symmetric Electric Quadrupole Interaction Hamiltonian</u>

If one combines equation (46) with the elements of the electric quadrupole interaction Hamiltonian matrix from equation (21), one obtains the interaction Hamiltonian matrix elements for the mixed case

$$H_{m,m} = -\omega_H \hbar m \delta_{m,m'} + \sqrt{\frac{\pi}{5}} \frac{C(I\,2\,I;\ m, 0, m)}{C(I\,2\,I;\ I, 0, I)} V_o^{(2)} eQ$$

$$H_{m,m\pm 1} = (-)^{\pm 1} \sqrt{\frac{\pi}{5}} \frac{C(I\,2\,I;\ m, \pm 1, m\pm 1)}{C(I\,2\,I;\ I, 0, I)} V_{\mp 1}^{(2)} eQ \tag{47}$$

$$H_{m,m\pm 2} = (-)^{\pm 2} \sqrt{\frac{\pi}{5}} \frac{C(I\,2\,I;\ m, \pm 2, m\pm 2)}{C(I\,2\,I;\ I, 0, I)} V_{\mp 2}^{(2)} eQ .$$

The location of the principal axes of the crystal (x', y', z'), the

direction of the magnetic field, and directions of the two detected gamma radiations $\vec{k}_1$ and $\vec{k}_2$ are shown in Figure 10.

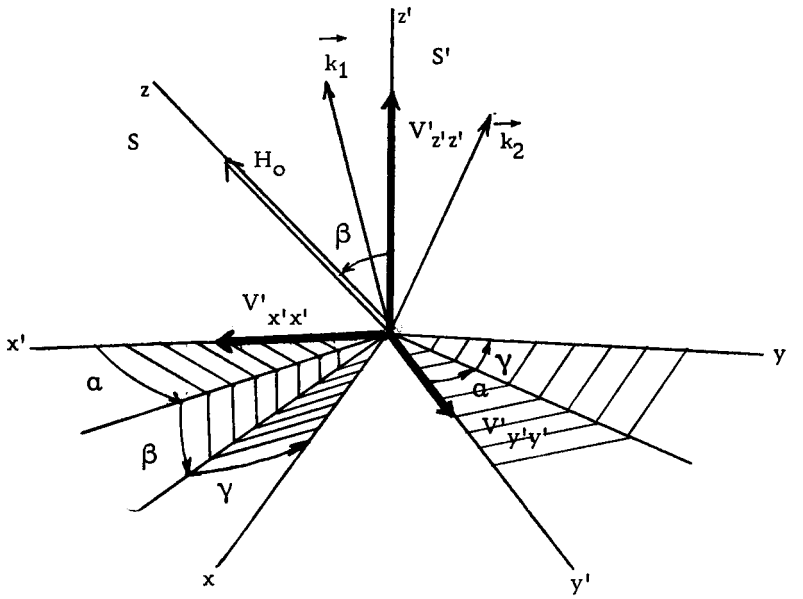

Figure 10. Arrangement of detected gamma radiations, magnetic field vector, and crystalline field gradients for $\eta \neq 0$, $y \neq 0$ case.

Since the direction of H_o is fixed in the laboratory, and since the crystals of a polycrystalline source may take on all possible directions relative to H_o as well as $\vec{k}_1$ and $\vec{k}_2$, the previously used technique of diagonalizing one Hamiltonian and averaging over all possible detector locations for each Q^* will no longer work. We will take the H_o-direction to be the quantization axis for the system. since the matrix elements of the magnetic interaction Hamiltonian are diagonal in a system (S) whose z-axis is parallel

to the direction of H_o. Writing the components $V_q^{(k)}$ in equation (47) in terms of the components $V_q^{(k)'}$ in the principal axis system of the crystal (S') by performing a rotation of coordinates one obtains

$$V_q^{(2)} = \sum_{\ell=-2}^{2} V_\ell^{(2)'} D_{\ell,q}^{(2)} \tag{48}$$

where the $D_{\ell,q}^{(2)}$ and their properties are given by Rose (29, p. 48-75).

The rotation of the S'-system through Euler angles α, β, and γ is done as follows:

1. Rotation perpendicular to z' through an angle α to bring x' into the plane containing H_o and z'.
2. Rotation about the new y-axis through angle β to make the z' axis collinear with the direction of H_o.
3. Rotation perpendicular to the z-axis through an angle γ.

Calculation of the $V_q^{(2)}$'s is rather tedious, and only the results are given here.

$$V_o^{(2)} = \frac{1}{8}\sqrt{\frac{5}{\pi}}\ (\eta \sin^2\beta \cos 2\alpha + 3\cos^2\beta - 1)\, V'_{z'z'}$$

$$V_{\pm 1}^{(2)} = \pm \frac{1}{8}\sqrt{\frac{30}{\pi}}\ V'_{z'z'} \sin\beta\, e^{\mp i\gamma} \left(\cos\beta \pm \frac{\eta}{6} e^{i2\alpha}[1 \mp \cos\beta] \mp \frac{\eta}{6} e^{-i2\alpha}[1 \pm \cos\beta]\right) \tag{49}$$

$$V_{\pm 2}^{(2)} = \frac{1}{16}\sqrt{\frac{30}{\pi}}\ V'_{z'z'} \left(\sin^2\beta + \frac{\eta}{6} e^{-i2\alpha}[1 \mp \cos\beta]^2 + \frac{\eta}{6} e^{i2\alpha}[1 \pm \cos\beta]^2\right) e^{\mp i2\gamma}$$

Evaluating the Clebsch-Gordan coefficients in equation (47) and substituting in the $V_q^{(2)}$'s from equation (49), we obtain the elements of a (2I + 1)-by-(2I + 1) Hermitian matrix

$$H_{m,m} = -\omega_H \hbar m + \omega_E \hbar \frac{1}{2}(3\cos^2\beta - 1 + \eta \sin^2\beta \cos 2\alpha)[3m^2 - I(I+1)]$$

$$H_{m,m\pm1} = \frac{3}{2}\omega_E \hbar \sin\beta \left(\cos\beta \mp \frac{\eta}{6}\left[(1\pm\cos\beta)e^{i2\alpha} - (1\mp\cos\beta)e^{-i2\alpha}\right]\right) e^{\pm i\gamma}(2m\pm1)[(I\mp m)(I\pm m+1)]^{\frac{1}{2}}$$

$$H_{m,m\pm2} = \omega_E \hbar \frac{3}{4}\left(\sin^2\beta + \frac{\eta}{6}\left[(1\pm\cos\beta)^2 e^{i2\alpha} + (1\mp\cos\beta)^2 e^{-i2\alpha}\right]\right) \times e^{\pm i2\gamma}[(I\pm m+2)(I\pm m+1)(I\mp m)(I\mp m-1)]^{\frac{1}{2}}.$$

For convenience, the elements of this matrix may be written in units of $\hbar\omega$. Defining $K_{m,m'} = \frac{H_{m,m'}}{\hbar\omega_E}$ and $y = \frac{\omega_H}{\omega_E}$ we obtain

$$K_{m,m} = -ym + \frac{1}{2}(3\cos^2\beta - 1 + \eta\sin^2\beta\cos 2\alpha)[3m^2 - I(I+1)]$$

$$K_{m,m\pm1} = \frac{3}{2}\sin\beta\left(\cos\beta \mp \frac{\eta}{6}\left[(1\pm\cos\beta)e^{i2\alpha} - (1\mp\cos\beta)e^{-i2\alpha}\right]\right) \times e^{\pm i\gamma}(2m\pm1)[(I\mp m)(I\pm m+1)]^{\frac{1}{2}} \tag{50}$$

$$K_{m,m\pm2} = \frac{3}{4}\left(\sin^2\beta + \frac{\eta}{6}\left[(1\pm\cos\beta)^2 e^{i2\alpha} + (1\mp\cos\beta)^2 e^{-i2\alpha}\right]\right) \times e^{\pm i2\gamma}[(I\pm m+2)(I\pm m+1)(I\mp m)(I\mp m-1)]^{\frac{1}{2}}.$$

For the polycrystalline case, one must compute

$$\overline{G^{s_1 s_2}_{\nu_1 \nu_2}(t)}^{\alpha,\beta,\gamma} = \frac{1}{8\pi^2} \int_{\alpha=0}^{2\pi} \int_{\beta=0}^{\pi} \int_{\gamma=0}^{2\pi} G^{s_1 s_2}_{\nu_1 \nu_2}(t)\, d\alpha \sin\beta\, d\beta\, d\gamma$$

which implies that the eigenvalues and elements of the rotation matrix in equation (14) must be found for every angle over the range of integration.

If one writes the secular equation for the Hamiltonian matrix, it will be seen that since the γ dependence of $H_{m,m'}$ occurs only in the form $e^{i\gamma(m-m')}$, no γ-dependent factors are present and so the eigenvalues E are independent of γ. The elements of the unitary matrix may then be expressed $\langle I_i m_i | U(\alpha,\beta) | I_i m_k \rangle e^{i m_k \gamma}$. This result is to be expected due to the axial symmetry of H. Equation (14) now takes the form

$$\begin{aligned} G^{s_1 s_2}_{\nu_1 \nu_2}(t) = \sum_{m_z, m_z'} \sum_{m_b, m_b''} & (-)^{m_b + m_b'' - 2I_b} C(I_b I_b \nu_1; m_b, -m_b', s_1) \\ & \times C(I_b I_b \nu_2; m_b'', -m_b''', s_2) \langle I_b m_z | U(\alpha,\beta) | I_b m_b'' \rangle^* \\ & \times \langle I_b m_z | U(\alpha,\beta) | I_b m_b \rangle \langle I_b m_z' | U(\alpha,\beta) | I_b m_b''' \rangle \\ & \times \langle I_b m_z' | U(\alpha,\beta) | I_b m_b' \rangle^* e^{-i/\hbar (E_{m_z} - E_{m_z'})t} \\ & \times e^{i\gamma(m_b - m_b' - m_b'' + m_b''')} . \end{aligned} \tag{51}$$

Averaging $G^{s_1 s_2}_{\nu_1 \nu_2}(t)$ over all γ, one finds that $m_b - m_b' = m_b'' - m_b'''$, or $s_1 = s_2 = s$, so that equation (51) takes the form

$$\overline{G^{s}_{\nu_1 \nu_2}(t)}^{\gamma} = \sum_{m_z, m_z'} \sum_{m_b, m_b''} (-)^{m_b + m_b'' - 2I_b} C(I_b I_b \nu_1; m_b, -m_b', s)$$

$$\times\ C(I_b I_b \nu_2; m_b'', -m_b''', s) < I_b m_z | U(\alpha, \beta) | I_b m_b'' >^{*} \tag{52}$$

$$\times\ < I_b m_z | U(\alpha, \beta) | I_b m_b > < I_b m_z' | U(\alpha, \beta) | I_b m_b''' >$$

$$\times\ < I_b m_z' | U(\alpha, \beta) | I_b m_b' >^{*} e^{-i/\hbar (E_{m_z} - E_{m_z'}) t}.$$

The following symmetry relations are valid (21, p. 248):

$$\overline{G^{-s_1, -s_2}_{\nu_1 \nu_2}}^{\gamma} = \overline{G^{s_1 s_2 *}_{\nu_1 \nu_2}}^{\gamma}$$

$$\overline{G^{s_2 s_1}_{\nu_2 \nu_1}(\pi - \alpha)}^{\gamma} = \overline{G^{s_1 s_2}_{\nu_1 \nu_2}(\alpha)}^{\gamma} \tag{53}$$

$$\overline{G^{s_1 s_2}_{\nu_1 \nu_2}(-y)}^{\gamma} = \overline{G^{s_1 s_2 *}_{\nu_1 \nu_2}(y)}^{\gamma}.$$

Making use of these, the integral over α and β is

$$\overline{G^{s_1 s_2}_{\nu_1 \nu_2}}^{\alpha\beta\gamma}(t) = \frac{1}{4\pi} \int_{\alpha=0}^{2\pi} \int_{\beta=0}^{\pi} \overline{G^{s_1 s_2}_{\nu_1 \nu_2}}^{\gamma}(t)\, d\alpha \sin\beta\, d\beta$$

$$= \frac{-8}{4\pi} \int_{\alpha=0}^{\pi/2} \int_{\cos\beta=1}^{0} \overline{G^{s_1 s_2}_{\nu_1 \nu_2}}^{\gamma}(t)\, d\alpha\, d(\cos\beta) \text{ for } s_1 = s_2 \tag{54}$$

$$= \frac{-4}{4\pi} \int_{\alpha=0}^{\pi} \int_{\cos\beta=1}^{0} \overline{G^{s_1 s_2}_{\nu_1 \nu_2}}^{\gamma}(t)\, d\alpha\, d(\cos\beta) \text{ for } s_1 \neq s_2 .$$

Dividing $\overline{G^{s_1 s_2}_{\nu_1 \nu_2}}^{\alpha\beta\gamma}$ into its real and imaginary parts, one has[2]

$$\overline{G^{s_1 s_2}_{\nu_1 \nu_2}}^{\alpha\beta\gamma} = a^{s}_{\nu_1 \nu_2} + i\, b^{s}_{\nu_1 \nu_2} . \tag{55}$$

Substituting into equation (6), we obtain for the correlation probability

$$W(\theta, t) = \sum_{\substack{\nu_1, \nu_2 \\ s}} (-)^s \left(a^{s}_{\nu_1 \nu_2}(t) + i b^{s}_{\nu_1 \nu_2}(t)\right) D^{\nu_1}_{s,0}(\alpha_1 \beta_1 0)$$

$$\times\, D^{\nu_2}_{-s,0}(\alpha_2 \beta_2 0)\, B_{\nu_1}(\gamma_1)\, B_{\nu_2}(\gamma_2) . \tag{56}$$

---

[2] The $a^{s}_{\nu_1 \nu_2}$ and $b^{s}_{\nu_1 \nu_2}$ in this thesis are not numerically the same as the $a^{\mu}_{k_1 k_2}$ and $b^{\mu}_{k_1 k_2}$ derived by Matthias <u>et al</u>. in reference (22). This difference comes from a difference between the definitions of their perturbation factor and the one used here.

For the case where the plane of the detector is perpendicular to the magnetic field

$$W_{\perp}(\theta, t) = \sum_{\substack{\nu_1, \nu_2 \\ s}} (-)^s \left(a^s_{\nu_1\nu_2}(t) + i\, b^s_{\nu_1\nu_2}(t)\right) \left(\frac{4\pi}{2\nu_1+1}\right)^{\frac{1}{2}} \left(\frac{4\pi}{2\nu_2+1}\right)^{\frac{1}{2}}$$

$$\times\, Y^{\,s}_{\nu_1}(\pi/2, \alpha_1)\, Y^{\,-s}_{\nu_2}(\pi/2, \alpha_2)\, B_{\nu_1}(\gamma_1)\, B_{\nu_2}(\gamma_2)$$

$$= \sum_{\substack{\nu_1, \nu_2 \\ s}} (-)^s \left(a^s_{\nu_1\nu_2}(t) + i\, b^s_{\nu_1\nu_2}(t)\right) \left(\frac{4\pi}{2\nu_1+1}\right)^{\frac{1}{2}} \left(\frac{4\pi}{2\nu_2+1}\right)^{\frac{1}{2}}$$

$$\times\, Y^{\,s}_{\nu_1}(\pi/2, 0)\, Y^{\,-s}_{\nu_2}(\pi/2, 0)\, e^{is(\alpha_1-\alpha_2)}\, B_{\nu_1}(\gamma_1) B_{\nu_2}(\gamma_2)$$

$$= \sum_{\substack{\nu_1, \nu_2 \\ s}} B_{\nu_1}(\gamma_1)\, B_{\nu_2}(\gamma_2)\, N^{\,s}_{\nu_1\nu_2}\, e^{is(\theta)} \left(a^s_{\nu_1\nu_2}(t) + i\, b^s_{\nu_1\nu_2}(t)\right) \tag{57}$$

where

$$N^{\,s}_{\nu_1\nu_2} = (-)^s Y^{\,s}_{\nu_1}(\pi/2, 0)\, Y^{\,-s}_{\nu_2}(\pi/2, 0) \tag{58}$$

$$= (-)^{\frac{\nu_1+\nu_2}{2}+s} \frac{\left[(2\nu_1+1)(2\nu_2+1)(\nu_1-s)!(\nu_2-s)!(\nu_1+s)!(\nu_2+s)!\right]^{\frac{1}{2}}}{4\pi(\nu_1-s)!!(\nu_2-s)!!(\nu_1+s)!!(\nu_2+s)!!}$$

for s even and

$= 0$ for s odd

and $\theta = \alpha_1 - \alpha_2$.

Finally we get

$$W_{\perp}(\theta, t) = \sum_{\substack{\nu_1, \nu_2 \\ s}} B_{\nu_1}(\gamma_1) B_{\nu_2}(\gamma_2) N^{s}_{\nu_1 \nu_2} \left(a^{s}_{\nu_1 \nu_2}(t) \cos s\theta - b^{s}_{\nu_1 \nu_2}(t) \sin s\theta\right) \quad (59)$$

for the probability function in the case of mixed magnetic dipole and electric quadrupole interactions with asymmetry not equal to zero. This expression may also be written

$$W_{\perp}(\theta, t) = \sum_{\substack{\nu_1, \nu_2 \\ s}} B_{\nu_1}(\gamma_1) B_{\nu_2}(\gamma_2) N^{s}_{\nu_1 \nu_2} \sqrt{a^{s^2}_{\nu_1 \nu_2} + b^{s^2}_{\nu_1 \nu_2}} \cos\left[s(\theta - \Delta\theta^{s}_{\nu_1 \nu_2})\right] \quad (60)$$

where

$$s\,\Delta\theta^{s}_{\nu_1 \nu_2} = \tan^{-1} \frac{b^{s}_{\nu_1 \nu_2}}{a^{s}_{\nu_1 \nu_2}} \quad (61)$$

which indicates that the correlation pattern is shifted in a plane perpendicular to the direction of the magnetic field as y is varied. As in previous cases, ν_{max} is limited to the smallest of integers $2I_b$, $2L_1$, and $2L_2$ by the same arguments as presented on page 10. From the properties of the Clebsch-Gordan coefficients in equation (52), it is obvious that the largest value of s will be equal to the smallest of integers ν_1 and ν_2.

From the first of equations (53) we see that $a^{s}_{\nu_1 \nu_2} = a^{-s}_{\nu_1 \nu_2}$ and $b^{s}_{\nu_1 \nu_2} = -b^{-s}_{\nu_1 \nu_2}$. One can also show that all terms with ν_1

or $\nu_2=0$ vanish. To do this write equation (52) with $\nu_2=0$ and making use of equation (3. 16c) of Rose (29, p. 38)

$$G^{0}_{\nu_1 0}(t) = \sum_{m_z, m_z'} \sum_{m_b, m_b''} \frac{(2\nu_1+1)^{\frac{1}{2}}}{2I_b+1} C(I_b \nu_1 I_b; m_b, 0, m_b')$$

$$\times\ C(I_b\, 0\, I_b; m_b'', 0, m_b''') < I_b m_z | U(\alpha, \beta) | I_b m_b''>^{*}$$

$$\times\ < I_b m_z | U(\alpha, \beta) | I_b m_b > < I_b m_z' | U(\alpha, \beta) | I_b m_b''' > \tag{62}$$

$$\times\ < I_b m_z' | U(\alpha, \beta) | I_b m_b' >^{*} e^{-i/\hbar (E_{m_z} - E_{m_z'})t}$$

but

$$C(I_b\, 0\, I_b;\ m_b'', 0, m_b''') = \delta_{m_b'', m_b'''} .$$

The sum $\sum_{m_b''} < I_b m_z | U(\alpha, \beta) | I_b m_b''>^{*} < I_b m_z' | U(\alpha, \beta) | I_b m_b''>$

is equal to $\delta_{m_z, m_z'}$ so

$$G^{0}_{\nu_1 0}(t) = \sum_{m_b} \frac{(2\nu_1+1)^{\frac{1}{2}}}{2I_b+1} C(I_b \nu_1 I_b;\ m_b, 0, m_b')$$

$$\times \sum_{m_z} < I_b m_z | U(\alpha, \beta) | I_b m_b > < I_b m_z | U(\alpha, \beta) | I_b m_b' >^{*}.$$

For the sum over m_z, we get $\delta_{m_b m_b'}$ leaving us with

$$G^{0}_{\nu_1,0}(t) = \sum_{m_b} \frac{(2\nu_1+1)^{\frac{1}{2}}}{2I_b+1} C(I_b \nu_1 I_b;\ m_b, 0, m_b').$$

Multiplying by $C(I_b 0 I_b;\ m_b;\ 0, m_b') = \delta_{m_b, m_b'}$

$$G^{0}_{\nu_1,0}(t) = \sum_{m_b} \frac{(2\nu_1+1)^{\frac{1}{2}}}{2I_b+1} C(I_b \nu_1 I_b; m_b, 0, m_b') C(I_b 0 I_b; m_b, 0, m_b')$$

$= \delta_{\nu_1,0}$ since it can be shown from the properties of Clebsch-Gordon coefficients that

$$\sum_{m_b} C(I_b 0\ I_b;\ m_b, 0, m_b')\ C(I_b 0 I_b; m_b, 0, m_b') = \frac{2I_b+1}{(2\nu_1+1)^{\frac{1}{2}}}$$

and so the $a^{s}_{\nu_1\nu_2}$ and $b^{s}_{\nu_1\nu_2}$ with $\nu_1=0$, $\nu_2\neq 0$ or $\nu_1\neq 0, \nu_2=0$ vanish. Note also that $G^{0}_{0,0} = a^{0}_{0,0} = 1$.

Calculation of Anisotropy for the Mixed Case

A(x) was calculated from Fortran IV programs using an I.B.M. 7040-7094 computer. Two programs were used for this calculation:

1. program for generation of perturbation factors $a^{s}_{\nu_1\nu_2}$ and $b^{s}_{\nu_1\nu_2}$.

2. program for calculating $A(\theta, x)$ from $a^{s}_{\nu_1\nu_2}$ with solid angle corrections as well as folds to account for finite time resolution of the apparatus and the distribution of frequencies ω_E over the nuclear locations.

In the first program, the averaging process described by equations (54) was performed by the method of Simpson to obtain $a^{s}_{\nu_1\nu_2}$ and $b^{s}_{\nu_1\nu_2}$ for each value of x and y used in the A(x) calculation. The Hamiltonian matrix elements in equation (50) were computed for each α-β pair used in the integration. Each matrix was diagonalized using the modified Jacobi method to find the eigenvalues and elements of the unitary matrix for the α-β pair. These eigenvalues and matrix elements were then used to compute the intgrands $G^{s}_{\nu_1\nu_2}$ from equation (52). Intervals of $\Delta \cos\beta = -0.10$ and $\Delta\alpha = 18^{o}$ were selected to achieve good accuracy with a reasonable amount of computer time. The program was checked by making calculations of A(x) for the $\eta = 0.3, y=0$ case and comparing them with those computed from the $y = 0$ program described previously and by comparing calculations for the $\eta = 0.3, y=3.0$ case made by Matthias et al. (21).

A discussion of the derivation of the expression for $W(\theta, t)$ with solid angle corrections for this case is found in the appendix.

The time resolution of the apparatus was taken into account by performing the convolution integral

$$\overline{W(\theta, t)} = \int W(\theta, t)\ \rho\ (T - t)\ dt$$

just as in the $\eta \neq 0, y = 0$ case.

The frequency distribution was taken into account by performing the integration

$$\overline{a^{s}_{\nu_1\nu_2}(y_o, t)} = \frac{\int a^{s}_{\nu_1\nu_2}(y, \omega_E t)\ P(\omega_E - \omega_E^{o})\, d\omega_E}{\int P(\omega_E - \omega_E^{o})\, d\omega_E} \tag{63}$$

where $P(\omega_E - \omega_E^{o})\, d\omega_E = \frac{1}{\sigma\sqrt{2\pi}}\, e^{-[(\omega_E - \omega_E^{o})^2/2\sigma^2]}\, d\omega_E$ as before. y_o is the ratio ω_H/ω_E^{o}, ω_H being the Larmor frequency for the applied magnetic field H_o. The frequency fold is complicated by the fact that $a^{s}_{\nu_1\nu_2}$ is dependent on ω_E through the parameter y. A detailed discussion of the frequency fold is found in the appendix.

Experimental Measurements

A differential angular correlation experiment similar to that described previously was performed on the 133-482 kilovolt cascade of Hf^{181} with external fields of 4.8 and 8.3-kilogauss applied to the polycrystalline source and perpendicular to the plane of the detectors.

The 8.3-kilogauss field was obtained by attaching 3/8 inch diameter pole pieces to a magneton magnet. A 0.205-inch gap was used. Small depressions in the pole faces were used to hold the source capsule, which was the same one used for the $y = 0$ experiment described before. The 4.8-kilogauss field was obtained

by generous shimming of the magnetron magnet to produce a long air gap in the magnetic circuit.

The fields were measured by means of a R. F. L. Model 1890 gaussmeter which operates on the Hall principle. This gaussmeter is claimed to have an accuracy of ± 3% by the manufacturer.

The fields were checked for fringing effects by measuring H_o as a function of probe paddle angle with the direction of the axis of the magnet. A nearly sinusoidal plot was obtained indicating that there was little fringing of the field.

It was necessary to provide magnetic shielding for the photomultiplier tubes. Using the old 6810A system, it was found that, with shielding provided by a Conetic shield which extended out to the leading edge of the NaI(Tl) crystal, adverse effects were noticed at a flux density of about 30 Gauss at the leading edge.

Each of the new 56AVP tubes was surrounded by several layers of Conetic AA shielding. This shielding was then enclosed in a 1/8-inch thick Shelby steel cylinder which extended 2-1/2 inches beyond the cathode. This served not only as a housing for the tube, but supported a 2-1/2 inch light pipe. The NaI(Tl) crystal was held in place by a 1-1/2 inch long aluminum cap which was threaded to the Shelby steel cylinder. The steel housing was designed in sections in order to either accommodate light pipes of various lengths, or allow operation with no light pipe at all.

The 8.3 kilogauss experiment was run for about 100 hours at each angle, with about 80,000 counts in the peak channel at each angle. The 4.8 kilogauss experiment was run about 112 hours at each angle with about 70,000 counts in the peak channels. True-to-chance ratios of about 80:1 were obtained in the peak channels for both of these experiments. The data were processed on the O.S.U. 1410 computer which computed the accidental subtraction, normalized to the product of the singles, and calculated the statistical errors for each data point.

Results and Conclusions

Figures 13 and 14 show the results of comparisons between the experimental points and those obtained from computer calculations using an $\eta = 0$, $y \neq 0$ program. Although the experimentally determined and the calculated peaks occur at approximately the same x values, the fit is not very good when amplitudes are compared. Although solid angle and prompt resolution corrections were made, the frequency distribution in ω_E was not taken into account. A more satisfactory fit would have been obtained if this correction had been added.

Figures 15 and 16 show experimentally determined points with applied fields of 4.8 kilogauss and 8.3 kilogauss and calculations made with the $\eta \neq 0$, $y \neq 0$ program described in this chapter. The

value of η used in the program was determined by the zero-field experiment to be 0.30, and the frequency distribution is the same 10% guassian used in that case. The values of y_o corresponded to the magnitude of the applied magnetic field. Evidently the theory matches the experimental results quite well considering the number of variables involved.

Alder et al. (3) have suggested that one might make use of their theory to find nuclear magnetic moments using solid sources. Such an experiment would have an advantage over the ordinarily used liquid source experiments by allowing one to use much higher specific activities and hence smaller source sizes. While the integral perturbation factors are very insensitive to y, the differential factors are rather sensitive, becoming increasingly so as x increases. In performing the frequency fold, 14 curves of A(x) were calculated in increments of $\Delta(\frac{y}{y_o}) = 0.110$ for the region $0.460 \leq y \leq 1.476$. As shown in Figures 11 and 12 these curves change noticeably in structure as y changes, and one would hope to be able to determine nuclear magnetic moments for this nucleus by fitting these curves to experimental results. Unfortunately, as shown in Figures 15 and 16, the structure is almost entirely removed when the various corrections are applied to the theory. The frequency distribution in ω_E has the most undesirable effect, since its "smearing" effect becomes more and more pronounced with increasing x, thereby destroying the structure

in the very region which is most sentitive to y. One also notes that even with little or no ω_E distribution statistics become worse with increasing x, thereby requiring that an experiment be run over a long period of time in order to obtain meaningful information at higher x-values. It is concluded that, in practice, it is impossible to measure magnetic moments using a solid source and magnetic interaction strength comparable to the electric quadrupole interaction strength, where there is a significant distribution of electric quadrupole interaction frequencies from nuclear site to nuclear site.

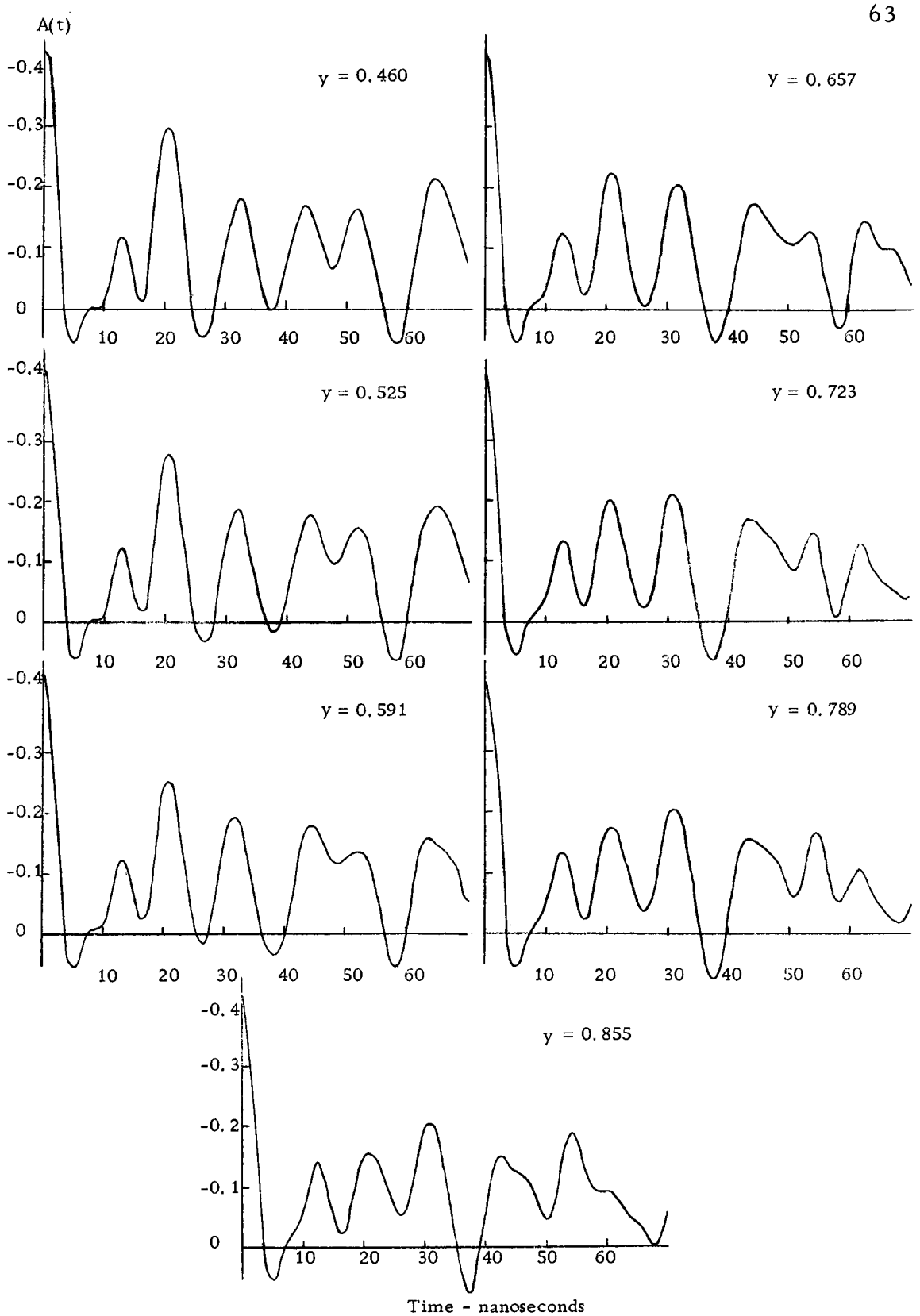

Figure 11. Theoretical values of anisotropy A(t) for an electric quadrupole interaction strength ω_o = 299 Mc/Sec. and asymmetry parameter $\eta = 0.30$ for $0.460 \leq y \leq 0.855$.

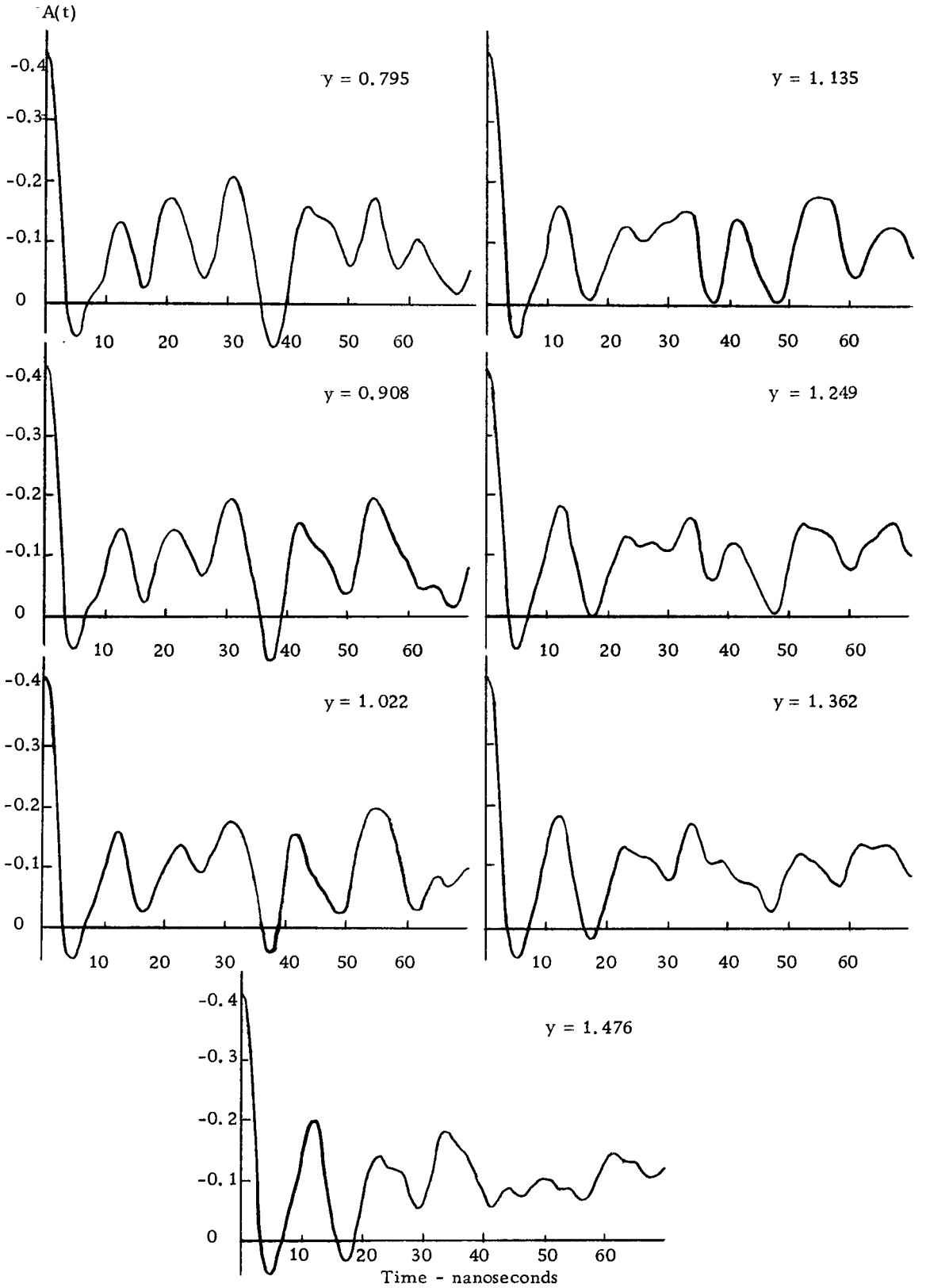

Figure 12. Theoretical values of anisotropy A(t) for an electric quadrupole interaction strength of 299 Mc/Sec and asymmetry parameter $\eta = 0.30$ for $0.795 \leq y \leq 1.476$.

Figure 13. Time dependent anisotropy of the 133-482 kilovolt gamma cascade in polycrystalline hafnium metal with applied magnetic field of 4.8 kilogauss. The dashed curve represents the uncorrected theory for asymmetry parameter $\eta = 0$ and $y = \frac{\omega_H}{\omega_E} = 0.585$ and the solid curve represents the same theory with corrections for solid angles subtended by the detectors as well as the prompt response of the spectrometer.

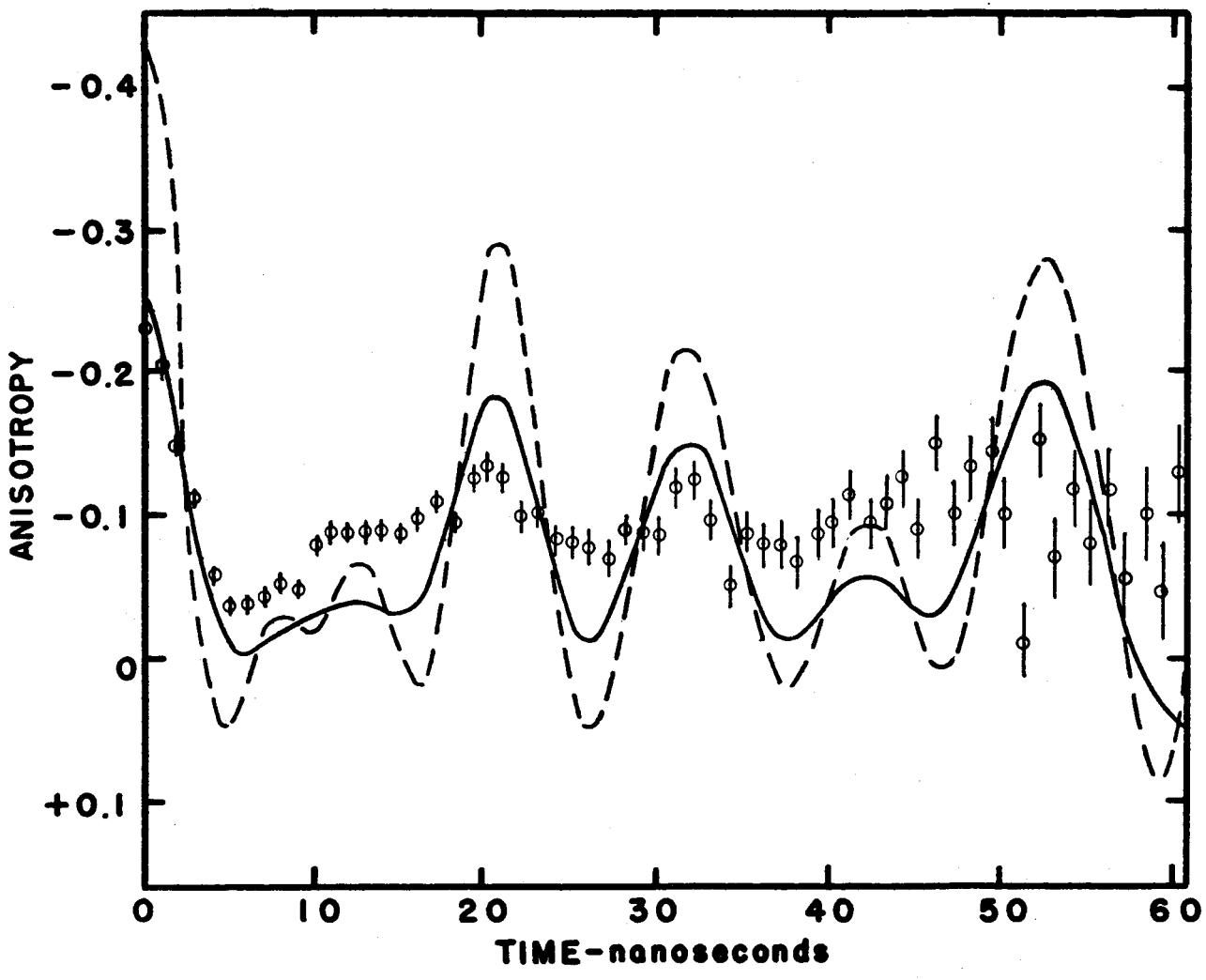
ANISOTROPY
-0.4
-0.3
-0.2
-0.1
0
+0.1
0
10
20
30
40
50
60
TIME-nanoseconds

Figure 14. Time dependent anisotropy of the 133-482 kilovolt gamma cascade in polycrystalline hafnium metal with applied magnetic field of 8.3 kilogauss. The dashed curve represents the uncorrected theory for asymmetry parameter $\eta = 0$ and $y = \frac{\omega_H}{\omega_E} = 0.877$ and the solid curve represents the same theory with corrections for solid angles subtended by the detectors as well as the prompt response of the spectrometer.

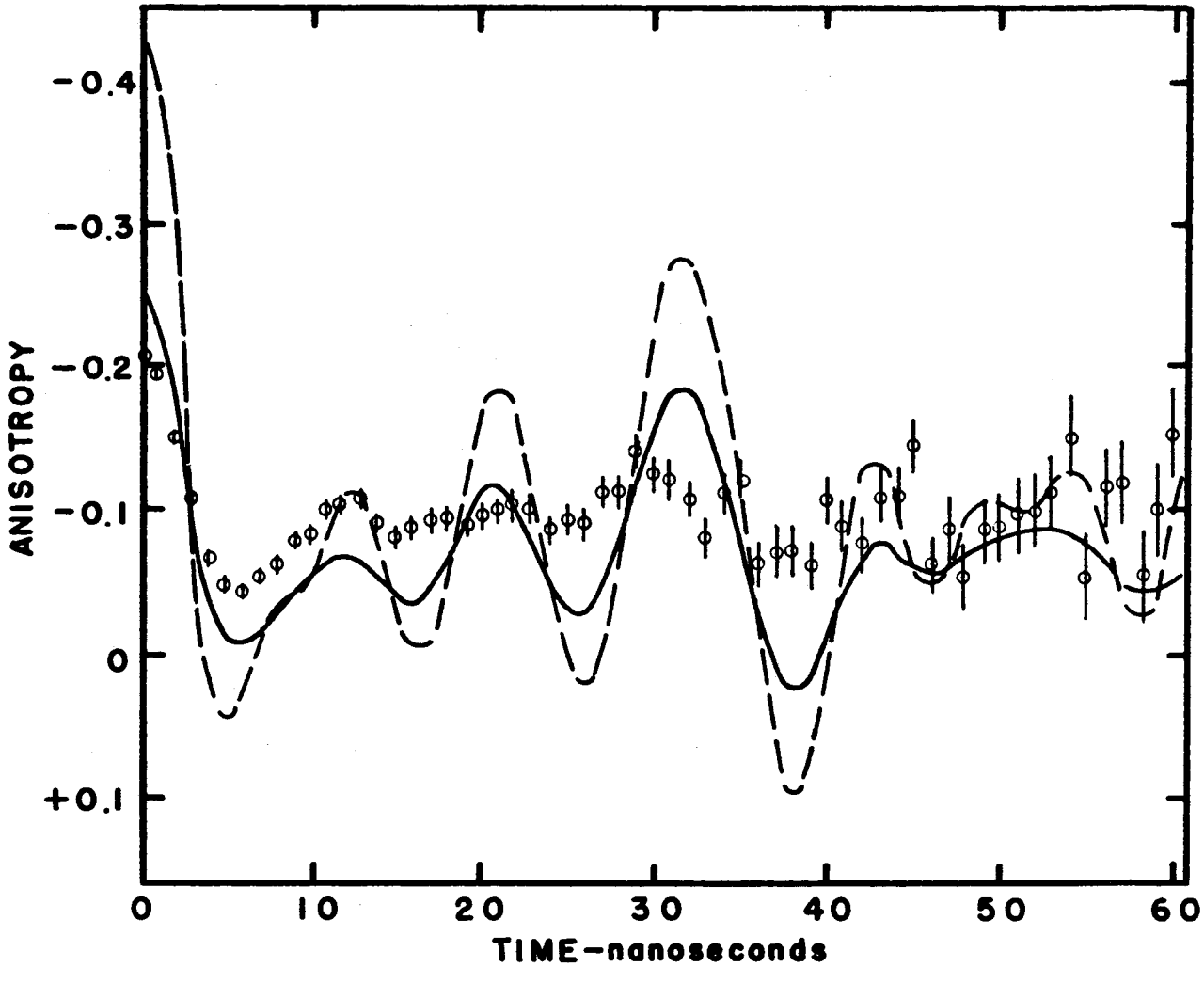
ANISOTROPY
-0.4
-0.3
-0.2
-0.1
0
+0.1
0
10
20
30
40
50
60
TIME-nanoseconds

Figure 15. Time dependent anisotropy of the 133-482 kilovolt gamma cascade in polycrystalline hafnium metal with applied magnetic field of 4.8 kilogauss. The dashed curve represents the uncorrected theory for asymmetry parameter $\eta = 0.30$ and $y = 0.591$ and the solid curve represents the same theory with corrections for solid angles subtended by the detectors as well as the prompt response of the spectrometer and a gaussian distribution in ω_E of width $\delta = 10\%$.

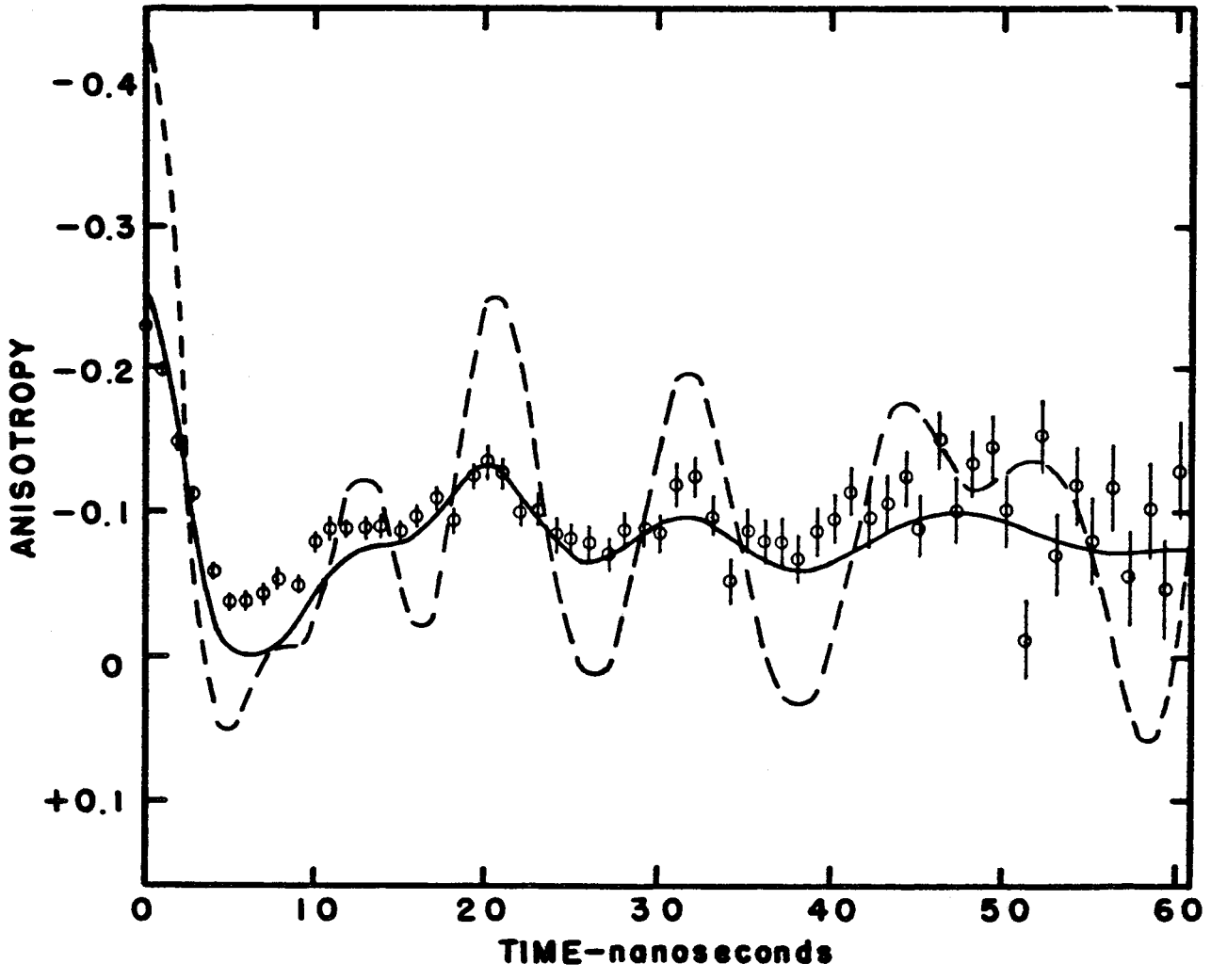
ANISOTROPY
-0.4
-0.3
-0.2
-0.1
0
+0.1
0
10
20
30
40
50
60
TIME-nanoseconds

Figure 16. Time dependent anisotropy of the 133-482 kilovolt gamma cascade in polycrystalline hafnium metal with applied magnetic field of 8.3 kilogauss. The dashed curve represents the uncorrected theory for assymetry parameter $\eta = 0.30$ and $y = 1.022$ and the solid curve represents the same theory with corrections for solid angles subtended by the detectors as well as the prompt response of the spectrometer and a gaussian distribution in ω_E of width $\delta = 10\%$.

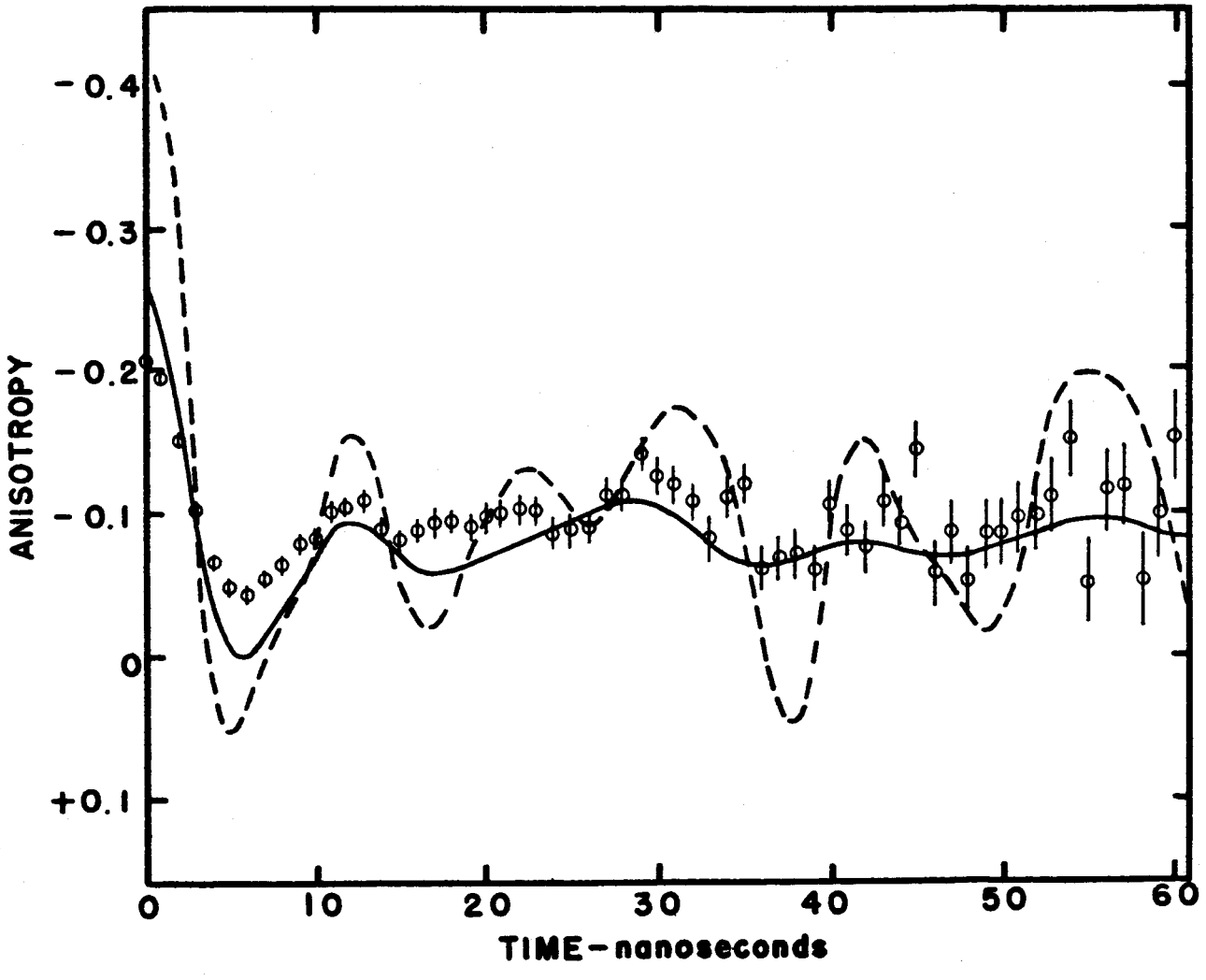
ANISOTROPY
-0.4
-0.3
-0.2
-0.1
0
+0.1
0
10
20
30
40
50
60
TIME-nanoseconds

BIBLIOGRAPHY

1. Abragam, A. and R. V. Pound. Influence of electric and magnetic fields on angular correlations. The Physical Review 92:943-962. 1953.

2. Alder, Kurt. Beitrage zur theorie der richtungskorrelation. Helvetica Physica Acta 25:235-251. 1952.

3. Alder, Kurt et al. Influence of a combined magnetic dipole and electric quadrupole interaction on angular correlations. The Physical Review 129:1199-1213. 1963.

4. Alder, Kurt et al. Study of nuclear structure by electromagnetic excitation with accelerated ions. Reviews of Modern Physics 28:432-542. 1956.

5. Bell, R. E. Coincidence techniques and the measurement of short mean lives. In: Alpha-, beta- and gamma-ray spectroscopy, vol. 2. Amsterdam, North Holland, 1965. p. 905-929.

6. Biedenharn, L. C. and M. E. Rose. Theory of angular correlations of nuclear radiations. Reviews of Modern Physics 25:729-777. 1953.

7. Bodenstedt, E. and J. D. Rogers. Magnetic moments of nuclear excited states. In: Perturbed angular correlations. Amsterdam, North-Holland, 1964. p. 93-151.

8. Cohen, M. H. Nuclear quadrupole spectra in solids. The Physical Review 96:1278-1284. 1954.

9. Cohen, S. G. et al. Measurement of the internal magnetic field acting on Ce-140 nuclei situated in ferromagnetic gadolinium and in lanthanum and cerium metal. In: Perturbed angular correlations. Amsterdam, North-Holland, 1964. p. 313-315.

10. Condon, E. U. and G. H. Shortley. The theory of atomic spectra. Cambridge, Cambridge University Press, 1963. 441 p.

11. Das, T. P. and M. Pomerantz. Nuclear quadrupole interactions in pure metals. The Physical Review 123:2070-2076. 1961.

12. Dean, C. Zeeman splitting in nuclear quadrupole resonance. The Physical Review 96:1053-1059. 1954.

13. Ferentz, M. and N. Rosenzweig. Table of F-coefficients. Lemont, Argonne National Laboratory, 1955. 133 p. (Argonne National Laboratory Report 5324(1955))

14. Frauenfelder, M. and R. M. Steffen. Angular distribution of nuclear radiation. In: Alpha-, beta- and gamma-ray spectroscopy, vol. 2. Amsterdam, North-Holland, 1965. 1742 p.

15. Fröberg, C. E. Introduction to numerical analysis. Reading, Addison-Wesley, 1965. 340 p.

16. Hinman, George W. et al. Angular correlation studies of electric field gradients in dilute silver alloys. The Physical Review 135:A206-A217. 1964.

17. Hinman, George W. et al. Influence of cold work and radiation damage on the angular correlation of gamma rays from In-111 nuclei embedded in silver. The Physical Review 135:A218-A220. 1964.

18. Hobson, E. W. The theory of spherical and ellipsoidal harmonics. New York, Chelsea Publishing Co., 1955. 500 p.

19. Lamarche, G. and G. M. Wolkoff. A theoretical investigation of the nuclear resonance absorbtion spectrum of Al-27 in spodumene. Canadian Journal of Physics 31:1010-1014. 1953.

20. Lehmann, P. and J. Miller. Influence de la capture K sur les correlations angulaires. Journal de Physique et le Radium 17:526-527. 1956.

21. Matthias, E. et al. Influence of a combined magnetic dipole and non-axially symmetric electric quadrupole interaction on angular correlations. Arkiv för Fysik 24:245-255. 1963.

22. Matthias, E. et al. Nuclear level splitting caused by a combined electric quadrupole and magnetic dipole interaction. The Physical Review 125:261-268. 1962.

23. Matthias, E. et al. Nuclear level splitting caused by a combined magnetic dipole and non-axially symmetric quadrupole interaction. Arkiv för Fysik 24:97-111. 1963.

24. Matthias, E. et al. Some remarks on static electric quadrupole perturbations in angular correlations. Physics Letters 4:41-43. 1963.

25. McGowan, F.K. and P.H. Stelson. Yields, angular distributions, and polarization of gamma rays from coulomb excitation. The Physical Review 109:901-916. 1958.

26. Merzbacher, Eugen. Quantum mechanics. New York, Wiley, 1961. 544 p.

27. Mottelson, B.R. and S.G. Nilsson. Classification of the nuclear states in deformed nuclei. The Physical Review 99:1615-1616. 1955.

28. Pound, R.V. Nuclear electric quadrupole interactions in crystals. The Physical Review 79:685-702. 1950.

29. Rose, M.E. Elementary theory of angular momentum. New York, Wiley, 1957. 248 p.

30. Rose, M.E. The analysis of angular correlation and angular distribution data. The Physical Review 91:610-615. 1953.

31. Schwarzschild, Arthur. Review of latest developments in delayed-coincidence measurements. In: Electromagnetic lifetimes and properties of nuclear states. Washington, National Academy of Sciences - National Research Council, 1962. p. 30-56.

32. Snyder, E.S. and Sherman Frankel. Decay of Hf-181. The Physical Review 106:755-764. 1957.

33. Sommerfeldt, R.W. and L. Schecter. Static quadrupole interaction in Ta-181. Physics Letters 3:5-6. 1962.

34. Sommerfeldt, R. W. Perturbed angular correlation in Ta-181. Ph. D. thesis. Corvallis, Oregon State University, 1964. 110 numb. leaves.

35. Stanford, A. L. Jr. and W. K. Rivers Jr. Angular correlation and angular distribution attenuation coefficients. Review of Scientific Instruments 30: 719-721. 1959.

36. Stelson, P. H. and F. K. McGowan. Gamma-ray yields from coulomb excitation. The Physical Review 99: 112-126. 1955.

37. Stelson, P. H. and F. K. McGowan. Polarization of gamma rays in Ta-181. The Physical Review 105: 1346-1349. 1957.

38. U. S. Atomic Energy Commission. The metallurgy of hafnium. Washington, U. S. Government Printing Office, 1960. 384 p.

39. Wilkner, E. G. and T. P. Das. Antishielding of nuclear quadrupole moments in heavy ions. The Physical Review 109: 901-916. 1958.

APPENDIX

APPENDIX

Frequency Fold for the Mixed Case

The frequency fold was done by performing the integration

$$\overline{a^{s}_{\nu_1\nu_2}(y_o, t)} = \frac{\int a^{s}_{\nu_1\nu_2}(y, \omega_E t)\, P(\omega_E - \omega_E^{o})\, d\omega_E}{\int P(\omega_E - \omega_E^{o})\, d\omega_E} \tag{A. 1}$$

where $P(\omega_E - \omega_E^{o})\, d\omega_E$ was chosen to be the Gaussian

$$\frac{1}{\sigma\sqrt{2\pi}}\, e^{-[(\omega_E - \omega_E^{o})^2/2\sigma^2]}\, d\omega_E .$$

But $y = \frac{\omega_H}{\omega_E} = \frac{\omega_H}{\omega_E^{o}} \frac{\omega_E^{o}}{\omega_E} = y_o \frac{\omega_E^{o}}{\omega_E} = y_o \frac{x_o}{x}$.

In terms of the parameter x then

$$\overline{a^{s}_{\nu_1\nu_2}(y_o, t)} = \frac{\int a^{s}_{\nu_1\nu_2}(y_o \frac{x_o}{x}, x)\, P(x - x_o)\, dx}{\int P(x - x_o)\, dx} \tag{A. 2}$$

where $x_o = \omega_E^{o} t$, so that one sees that for every x one must substitute $y = y_o \frac{x_o}{x}$ into the Hamiltonian and then proceed to calculate $a^{s}_{\nu_1\nu_2}$ for substitution into the integrand. The calculation was done by numerical integration on the 7040-7094 computer.

The Gaussian was limited to ordinate values of 0.01 of peak

value and above. This immediately limits $\frac{y}{y_o}$ to the range $0.76 \leq \frac{y}{y_o} \leq 1.44$. To facilitate this calculation, 175 $a^s_{\nu_1\nu_2}$ were calculated for each of seven values of y in the above range for each y_o. The 175 x 7 x 7 = 8575 values of $a^s_{\nu_1\nu_2}$ for each y_o were stored on magnetic tape as they were generated, and later stored in the computer memory for execution of the frequency fold. The computer selected appropriate $a^s_{\nu_1\nu_2}$ values from the memory depending on the calculated value of y for each x in equation (A. 2). Figure A1 shows a map of the region of $a^s_{\nu_1\nu_2}$ values computed. The dashed line is the locus of points calculated for one value of t. It required about 10 hours of 7094 time to calculate the perturbation factors for both values of y_o.

Derivation of $W(\theta, t)$ with Solid Angle Corrections

No Applied Magnetic Field

The expression for $W(\theta, t)$ for the case of a pure electric quadrupole interaction is

$$W(\theta, t) = \sum_{\nu} G_\nu A_\nu P_\nu(\cos\theta) = \sum_{\nu} G_\nu B_\nu(\gamma_1) B_\nu(\gamma_2) P_\nu(\cos\theta).$$

The 133-482 kilovolt cascade is a $\frac{1}{2}(E2)5/2(M1 + E2)7/2$ sequence. Since the second transition is mixed, the $B_\nu(\gamma_2)$ must be calculated from the expression (see reference 13).

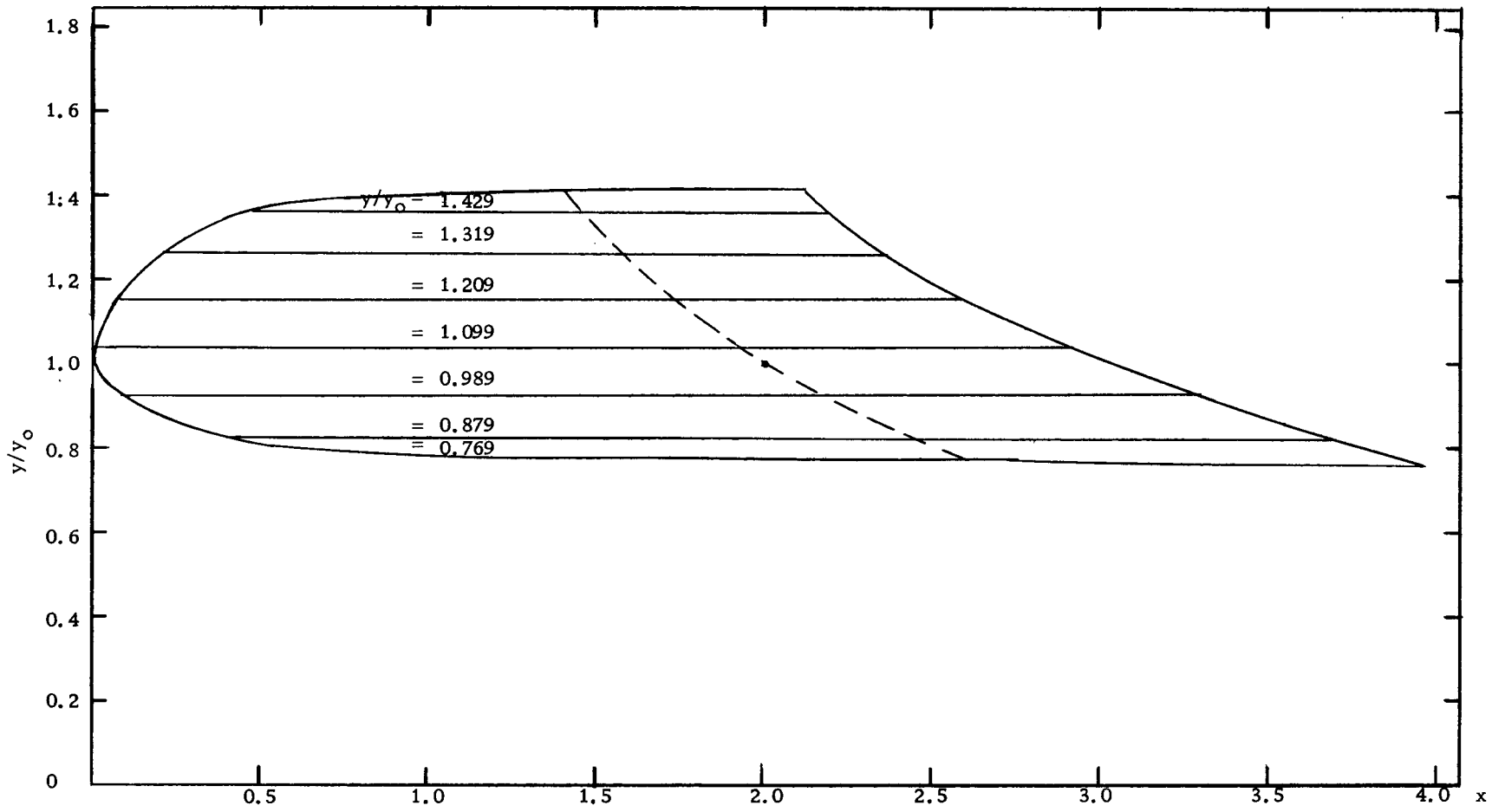

Figure A1. Map of ranges of y/y_o and x for which $a^s_{\nu_1 \nu_2}$ were calculated to make the frequency distribution fold for each y_o value. The dashed line represents the locus of points used in the fold for $x_o = 2$. The map is divided into zones representing the seven values of y/y_o for which a's were calculated.

$$B_\nu(\gamma_2) = F_\nu(L_2L_2I_cI_b) + \delta_2^2(\gamma)F_\nu(L_2'L_2'I_cI_b) + 2\delta_2(\gamma)F(L_2L_2'I_cI_b)$$

where $\delta_2^2(\gamma)$ is the ratio of the intensity of the L'-pole to that of the L-pole radiation. Snyder and Frankel (32) have found $\delta_2 = 6.2 \pm 0.3$ for this cascade. Using the F_ν values tabulated by Ferentz and Rosenzweig (13) we obtain $A_2 = -0.2880$ and $A_4 = -0.0704$.

For calculating solid angle corrections, one uses the method developed by Rose (30). The correction factors for the k-th radiation $\left(\frac{J_\nu}{J_o}\right)_k$ are multiplied in each term to obtain the solid angle corrected

$$\overline{W(\theta, t)} = \sum_\nu G_\nu \left(\frac{J_\nu}{J_o}\right)_k \left(\frac{J_\nu}{J_o}\right)_{k'} A_\nu P_\nu(\cos\theta) .$$

The $\left(\frac{J_\nu}{J_o}\right)_k$ factors for 1.5"-diameter NaI(Tl) crystals of various heights and for various gamma energies and source-to-detector distances are obtained from the curves of Stanford and Rivers (35). For the 133-482 kilovolt cascade and the source-to-detector distance of five centimeters used in our experiment, we find

$$\left(\frac{J_2}{J_o}\right)_{133} = 0.912$$

$$\left(\frac{J_2}{J_o}\right)_{482} = 0.931$$

$$\left(\frac{J_4}{J_o}\right)_{133} = 0.728$$

$$\left(\frac{J_4}{J_o}\right)_{482} = 0.770 .$$

Substituting into the expression for $W(\theta, t)$ we get

$$\overline{W(\theta, t)} = 1 - 0.2444\, P_2(\cos\theta)\, G_2(t) - 0.03963\, P_4(\cos\theta) G_4(t)$$

so that

$$\overline{W(\pi, t)} = 1 - 0.2444\, G_2(t) - 0.03963\, G_4(t)$$

and

$$\overline{W(\tfrac{\pi}{2}, t)} = 1 + 0.1222\, G_2(t) - 0.01486\, G_4(t).$$

Applied Magnetic Field

For the case of combined magnetic dipole and electric quadrupole interactions with the applied field perpendicular to the plane of the detectors, $W(\theta, t)$ is given by equation (59) as

$$W_\perp(\theta, t) = \sum_{\substack{\nu_1 \nu_2 \\ s}} B_{\nu_1}(\gamma_1)\, B_{\nu_2}(\gamma_2)\, N^s_{\nu_1\nu_2}\, (a^s_{\nu_1\nu_2}(t) \cos s\theta - b^s_{\nu_1\nu_2}(t) \sin s\theta).$$

For the $I = 5/2$ case, this expression may be written

$$\begin{aligned} W_\perp(\theta, t) = {} & A_{00} N^0_{00} a^0_{00} + A_{22} N^0_{22} a^0_{22} + (A_{24} + A_{42}) N^0_{24} a^0_{24} \\ & + A_{44} N^0_{44}\, a^0_{44} + [\, 2A^2_{22} N^2_{22} a^2_{22} + 2(A_{24} + A_{42}) N^2_{24} a^2_{24} \\ & + 2A_{44} N^2_{44} a^2_{44}]\, \cos 2\theta + 2A_{44} N^4_{44} a^4_{44} \cos 4\theta \end{aligned}$$

where $A_{\nu_1\nu_2} = B_{\nu_1}(\gamma_1)\, B_{\nu_2}(\gamma_2)$.

Since $A(t) = \frac{W(\pi, t)}{W(\pi/2, t)} - 1$ is insensitive to azimuthal shift, one notes from equations (60) and (61) that the $b^{s}_{\nu_1\nu_2}$ terms are zero for $W(\pi, t)$ and $W(\pi/2, t)$. Calculating $N^{s}_{\nu_1\nu_2}$ from equation (58) and the $A_{\nu_1\nu_2}$ as in the $y = 0$ case one obtains

$$A_{00} = 1$$

$$A_{22} = -0.2880 \qquad A_{44} = -0.0704$$

$$A_{24} = -0.0613 \qquad A_{42} = -0.3320$$

$$N^{0}_{00} = \frac{1}{4\pi} \qquad N^{0}_{44} = \frac{81}{256\pi}$$

$$N^{0}_{22} = \frac{5}{16\pi} \qquad N^{2}_{44} = \frac{45}{128\pi}$$

$$N^{2}_{22} = \frac{15}{32\pi} \qquad N^{4}_{44} = \frac{315}{512\pi}$$

$$\begin{aligned} W_{\perp}(\theta, t) = {} & 0.07958 - 0.02865\, a^{0}_{22} + 0.03937\, a^{0}_{24} - 0.00709\, a^{0}_{44} \\ & + (-0.08594\, a^{2}_{22} + 0.1016\, a^{2}_{24} - 0.01575\, a^{2}_{44}) \cos 2\theta \\ & - 0.02757\, a^{4}_{44} \cos 4\theta. \end{aligned}$$

In order to make solid angle corrections using available curves, the $\cos 2\theta$ and $\cos 4\theta$ terms may be written as expansions in $P_{\ell}(\cos\theta)$. From Hobson (18) one obtains the terminating expansion

$$\frac{2\cdot 3\cdot 5\cdot\cdot\cdot(2n+1)}{2\cdot 4\cdot\cdot\cdot 2n}\cos n\theta = (2n+1)\,P_n(\cos\theta)$$

$$+ (2n-3)\,\frac{n^2-(n+1)^2}{n^2-(n-2)^2}\,P_{n-2}(\cos\theta)+(2n-7)\,\frac{[n^2-(n+1)^2]\,[n^2-(n-1)^2]}{[n^2-(n-2)^2]\,[n^2-(n-4)^2]}$$

$$\times\; P_{n-4}(\cos\theta)\cdot\cdot\cdot$$

which gives

$$\cos 2\theta = \frac{4}{3}\,P_2(\cos\theta) - \frac{1}{3}\,P_0(\cos\theta)$$

$$\cos 4\theta = \frac{64}{35}\,P_4(\cos\theta) - \frac{16}{21}\,P_2(\cos\theta) - \frac{1}{15}\,P_0(\cos\theta).$$

Once more, the solid angle corrections to the P_ν terms are given by $\left(\frac{J_\ell}{J_o}\right)_k$ for the k-th radiation. The solid-angle corrected $W(\theta, t)$ is

$$\overline{W_\perp(\theta, t)} = 0.07958 - 0.02865\,a^0_{22} + 0.03937\,a^0_{24} - 0.00709\,a^0_{44}$$

$$+ (-0.08594\,a^2_{22} + 0.1016\,a^2_{24} - 0.01575\,a^2_{44})$$

$$\times\left[\frac{4}{3}\left(\frac{J_2}{J_o}\right)_{133}\left(\frac{J_4}{J_o}\right)_{482} P_2(\cos\theta) - \frac{1}{3}\right]$$

$$- (0.02757\,a^4_{44}\left[\frac{64}{35}\left(\frac{J_4}{J_o}\right)_{133}\left(\frac{J_4}{J_o}\right)_{482} P_4(\cos\theta)\right.$$

$$\left. - \frac{16}{21}\left(\frac{J_2}{J_o}\right)_{133}\left(\frac{J_2}{J_o}\right)_{482} P_2(\cos\theta) - \frac{1}{15}\right].$$

The final solid angle corrected expressions needed to compute anisotropy for the mixed case are

$$\overline{W_{\perp}(\pi, t)} = 0.07958 - 0.02865\, a_{22}^{0} - 0.06860\, a_{22}^{2} + 0.03936\, a_{24}^{0}$$

$$+ 0.08112\, a_{24}^{2} - 0.00712\, a_{44}^{0} - 0.01263\, a_{44}^{2} - 0.008634\, a_{44}^{4}$$

$$\overline{W_{\perp}(\tfrac{\pi}{2}, t)} = 0.07958 - 0.02865\, a_{22}^{0} + 0.07728\, a_{22}^{2} + 0.03936\, a_{24}^{0}$$

$$- 0.09138\, a_{24}^{2} - 0.00712\, a_{44}^{0} + 0.01423\, a_{44}^{2} - 0.01775\, a_{44}^{4}.$$